Mixed Quantum/Classical Molecular Dynamics Simulations of the Hydrated Dielectron: The Role of Exchange in Condensed–Phase Structure, Dynamics and Spectroscopy

Ross E. Larsen and Benjamin J. Schwartz*

Department of Chemistry and Biochemistry,

University of California,Los Angeles, CA 90095

(Dated: May 20, 2004)

Abstract

The importance of quantum mechanical exchange in determining the electronic properties of molecules has long been appreciated. Less attention has been paid, however, to how exchange affects the properties of quantum mechanical objects in the presence of a solvent. How important are spin statistics in determining the structure and dynamics of such objects? For instance, do fully solvent–supported single–electron states, such as solvated electrons, interact with each other in such a way that quantum mechanical exchange and correlation must be taken into account? That is, does the Pauli exclusion principle enhance or supress the formation of bound pairs of solvated electrons, so–called bipolarons, and what role does the solvent play? We have approached this question by performing mixed quantum/classical molecular dynamics simulations of two excess electrons solvated by bulk liquid water. The mixed quantum/classical dynamics is performed at the level of the Born–Oppenheimer approximation, so that the water motions obey classical mechanics and the electronic degrees of freedom evolve on the ground state adiabatic energy surface. The two–electron adiabatic eigenstates are calculated with full configuration interaction (CI) using a highly efficient real–space method that we have recently introduced [R. E. Larsen and B. J. Schwartz, *J. Chem. Phys.* **2003**, *119*, 7672] to compute the Coulomb and exchange interaction energies. Our calculations show that two excess electrons form *dielectrons*, that is, they are confined by the solvent to a single cavity for both singlet and triplet pairing of the electron spins. When the electrons' spins are singlet–paired, the dielectron is confined to an aspher-

ical, "potato–shaped" cavity, whereas when the electrons' spins are triplet–paired the dielectron occupies a "peanut–shaped" cavity. We find that in both cases water molecules in the first solvation shell solvate the hydrated dielectron by pointing one of their O–H bonds directly toward the charge, just as occurs with a single hydrated electron. We examine the time–evolution of various dielectron properties, and compare and contrast the dielectron dynamics with the dynamics of a single hydrated electron. Finally, taking advantage of the fact that our CI calculation generates both ground and excited states, we have computed the optical absorption spectra of both singlet and triplet dielectrons. We discuss the significance of the predicted optical absorption spectra for the possible direct spectroscopic observation of hydrated dielectrons.

I. INTRODUCTION

The properties of quantum mechanical objects dissolved in liquids are of great importance for understanding chemical reaction dynamics in solution. Charge transfer reactions, for instance, involve nontrivial changes in electronic structure (a fundamentally quantum mechanical construction), but the likelihood of these transfers can end up controlled by the largely classical dynamics and thermodynamics of the solvent.[1] This leads to a key question: how do the classical many–body dynamics of a solvent combine with the quantum dynamics of electrons to determine the physical properties of the quantum mechanical object? Much of the theoretical and simulation work aimed at answering this question has concentrated on the properties of an excess electron dissolved in a liquid.[2–8] From a theoretical viewpoint, a single solvated electron is the canonical case because it provides the simplest possible example of a quantum object interacting with a solvent.

In addition to being the simplest possible quantum solute, solvated electrons are ideal candidates for study because their properties are wholly determined by the solvent, and they will thus be acutely sensitive to the properties of the liquid in which they are dissolved. For instance, in non–polar solvents such as xenon, electrons occupy a rather large volume and are ultimately confined only by disorder–induced localization to a region typically spanning many atomic diameters.[4] Polar solvents, on the other hand, confine the electron to a much smaller region, and the electron consequently exerts a strong influence on its local

environment.[9] In this paper, we focus on electrons dissolved in the most important polar solvent, water. Early theories of the solvated electron in a polar solvent treated the solvent as a dielectric continuum,[3] but the subsequent use of path–integral methods[5] allowed molecular details of the solvent to be included in calculations of ground–state properties of the solvated electron. The zeroth–order picture that arose from these calculations is that the electron is a hydrophobic species that carves out a spherical cavity and is stabilized by polarization of the surrounding solvent: the eigenstates of the hydrated electron are roughly those of a particle in a finite spherical box. This picture is supported by mixed quantum/classical molecular dynamics simulations,[6,7] which have reproduced both the steady–state and ultrafast spectroscopic properties of the hydrated electron. In addition, recent resonance Raman spectra also provide strong support for the cavity model of the hydrated electron.[10]

One of the great appeals of treating the solvated elecron within a mixed quantum/classical (QM/CM) formalism is that there is only a single QM degree of freedom. Thus, the electronic properties are determined by a competition between the Heisenberg uncertainty principle, which drives the electron to spread out, and the solvent polarization, which responds to keep the electron localized. This simplicity, however, does not apply to more complex systems, such as those with more than one interacting electron, because of the challenge of correctly treating QM exchange and correlation. For example, there have been hints that QM exchange effects must be included to correctly treat electron detachment from (multi–electron) atoms dissolved in liquids,[11] but up to now there has been relatively little examination of how exchange effects manifest themselves in the context of liquid–phase solvation.[12]

In this paper, we will explore the role of exchange in the properties of solvated quantum objects by studying the simplest conceivable system that can show the effects of quantum mechanical exchange: two electrons dissolved in liquid water. One can envision two qualitatively different possibilities for how the two electrons might behave. The two electrons might repel each other and end up as two independent solvated electrons, thus minimizing their Coulomb repulsion at the expense of creating two cavities in the solvent. On the other hand, the hydrophobicity of the electrons might drive the two electrons into a single cavity, forming a bound bipolaron, even though the electrons strongly repel each other. In fact, early continuum calculations suggested that solvent polarization should be able to overcome the electron–electron Coulomb repulsion so that both electrons will occupy a single cavity,

forming what has been called either a bipolaron or *dielectron*.[15] In the early 1990s, this type of bipolaron formation was seen in Car–Parinello studies of excess electrons in NH_3,[13] as well as in simulations of electrons in molten KCl.[14] Moreover, spin density functional theory (DFT) calculations showed the existence of two distinct types of dielectron in water clusters.[24]

Although the DFT–based calculations suggest that bound dielectrons do exist in polar liquids,[13,14,24] the accuracy of the results, as with all DFT calculations, is limited by the choice of exchange–correlation functional. Furthermore, ground–state–only DFT–based calculations do not allow for the prediction of observables that depend on electronic excited states, such as the absorption spectrum, and thus such calculations have not been able to make contact with experiment. With recent advances in computer technology, we believe the time has come to revisit this model problem and explore the effects of QM exchange in condensed–phase dynamics. Thus, we study both spin–singlet and spin–triplet solvated dielectrons using mixed quantum/classical molecular dynamics. We solve the full two–electron quantum problem using our recently–introduced real–space configuration interaction (CI) with important states method.[16] The method is efficient enough to allow us to compute the electronic structure at every time step of a molecular dynamics trajectory, and because CI generates excited–state wavefunctions, the method also lets us make the first *ab initio* predictions of the absorption spectrum of this two–electron solvent–supported species.

The rest of this paper is organized as follows. In Section II, we discuss the model potentials and computational techniques used to calculate the mixed quantum/classical molecular dynamics of solvated dielectrons. Section III describes the equilibrium properties of both singlet–paired and triplet–paired dielectrons, focusing not only on the average energetic and geometric characteristics of the dielectron, but also on the dielectron dynamics. In Section IV we calculate the optical absorption spectrum of both singlet and triplet dielectrons and compare their spectra to the absorption spectrum of the (single) solvated electron. In addition, we discuss the implications the predicted absorption spectra have for earlier (disputed) claims of the direct experimental observation of dielectrons.[40–42] We close in Section V with a brief discussion of the importance of exchange and spin symmetry in condensed–phase reaction dynamics.

II. MODEL AND COMPUTATIONAL DETAILS

A. Simulation Details

Our simulations of the hydrated dielectron take place in a box 18.17 Å on a side containing 200 classical water molecules modelled using SPC–flex potentials,[17] and two QM electrons that interact with the water molecules via a pseudopotential derived by Schnittker and Rossky.[25] Although this pseudopotential does not agree with experiment as well as more modern versions,[20] we chose the Schnittker–Rossky form to allow direct comparison with the extensive computer simulations of the (single) hydrated electron that have been made with this model.[6,7] Minimum–image periodic boundary conditions were used for the classical solvent–solvent interactions.[26]

Our computational approach to the mixed QM/CM dynamics of the water–dielectron system uses what we have called the "real–space configuration–interaction with important states method." This method has been described in detail in a recent paper,[16] so in this Section we restrict ourselves to a brief review and a discussion of the computational details specific to the molecular dynamics simulations of the hydrated dielectron presented here. The Hamiltonian for two electrons is

$$\hat{H} \;=\; \hat{H}_1 + \hat{H}_2 + \hat{V}_{12} \;, \tag{1}$$

where $\hat{H}_i$ is the Hamiltonian for electron i (including the electron–solvent interaction) and $\hat{V}_{12}$ is the Coulomb interaction between the electrons. In CI, we expand the adiabatic dielectron wavefunctions in linear combinations of appropriately–symmetrized products of the single–electron adiabatic eigenstates,

$$|n,m\rangle_{\pm} \;=\; \left(|n>|m> \;\pm |m>|n>\right)/\sqrt{2} \;, \quad (m>n)$$

$$|n,n\rangle_{+} \;=\; |n>|n> \;, \tag{2}$$

where the states $\{|j>\}$ are single–electron eigenstates of $\hat{H}_1$ (or, equivalently, $\hat{H}_2$), the plus sign is used for spin singlet pairs and the minus sign when the spins are triplet paired, and in each product the first single–electron state is for electron 1 and the second for electron 2. Each dielectron eigenstate is thus written as $|\Psi_i>_{\pm} = \sum_{nm} c^{\pm\, i}_{n,m}|n,m>_{\pm}$, so that the two–electron eigenenergies, E_i, become a sum of single–electron adiabatic eigenenergies, plus

a sum of energies that come from computing the expectation value of the Coulomb potential using $|\Psi_i>_\pm$,

$$ {}_\pm<\Psi_i| \left(\frac{e^2}{r_{12}}\right) |\Psi_i>_\pm = \; V_c \; \pm \; V_{ex} \; , \tag{3} $$

where we call V_c the Coulomb energy and V_{ex} the exchange energy; explicit formulas for calculating V_c and V_{ex} using our real–space quadrature are given in Eqs. 8–10 of Ref. 16.

We compute the two electron wavefunctions for each solvent nuclear configuration by first using an iterative block–Lanczos procedure to find the adiabatic, single–electron eigenstates on a $16 \times 16 \times 16$ cubic grid. We then construct the two–electron eigenstates using configuration interaction (CI) as described above and in Ref. 16. The CI calculations reported here use a product basis constructed from all combinations of the lowest 10 single–electron eigenstates. This results in 55 spatially symmetric product basis states for the spin–singlet dielectron and 45 spatially anti–symmetric product basis states for the spin–triplet dielectron. To reduce the computational cost enough for molecular dynamics to be practical, we also make what we call the *important states* approximation.[16] The idea is to construct the full CI matrix infrequently (in this case, every $\tau_{update} = 3fs$) and determine which subset of product basis states make up 99.95% of the ground state ($f_{imp} = 0.9995$ in the notation of Ref. 16); for times between updates, only this subset of important product basis states is used for the CI calculation. Making this approximation reduces the average cost of solving for the dielectron eigenstates by 60% (see Table IV of Ref. 16).

All of the molecular dynamics calculations presented in this paper use the Born–Oppenheimer approximation, and the dielectron is restricted to be in the ground state at all times. The force exerted on the water molecules by the electrons is taken to be the Hellmann–Feynman (HF) force, which is calculated as described in the Appendix of Ref. 16. The nuclear positions and velocities are propagated in time using the velocity Verlet algorithm with a time step of 1 fs.[26] Our Hamiltonian does not include magnetic fields or other terms that could lead to mixing between singlet and triplet dielectronic states; this lack of mixing allows us to run separate spin–coherent singlet and triplet trajectories.

The results presented in Section III for the equilibrium properties of singlet and triplet dielectrons were taken from separate 30–ps trajectories for each spin mainfold. When run on a personal computer with an AMD Athlon XP 1700+ CPU, it took roughly one week to generate 3 ps of dynamics. The singlet dielectron trajectory was started from a configura-

tion that was generated by adding a second electron to an equilibrated hydrated–electron configuration and equilibrating with velocity rescaling for 3.5 ps. The initial triplet configuration was generated by taking an equilibrated spin–singlet configuration, changing the spin state and equilibrating for 2 ps. The average temperature for the 30–ps singlet run was 296 K, with a root–mean–squared (RMS) deviation of 11 K. For the triplet run, the average temperature was 293 K, with an RMS deviation of 11 K.[21] In order to compare dielectrons to the well–studied (single) hydrated electron, we also have run a 60–ps trajectory with a single electron confined to the ground state, with the same simulation conditions, time step, and grid size as for the dielectron runs.

B. Characterization of the dielectron

Our study of dielectrons includes an examination of their shape and size. We will characterize dielectron geometries using the total charge density, which is what determines the force the dielectron exerts on the water molecules. This is most easily accomplished by computing various moments of the two–electron density, $\rho^{(2)}(\mathbf{r})$. We have displayed the explicit form that this two–electron distribution takes with the CI expansion in Ref. 16, except that here for convenience we normalize the density so that $\int d\mathbf{r}\rho^{(2)}(\mathbf{r}) = 1$, rather than 2. The average "size" of the dielectron is given by the radius of gyration, R_{gyr}, defined by,

$$R_{gyr}^2 = \int d\mathbf{r}\rho^{(2)}(\mathbf{r})|\mathbf{r}|^2 \ , \tag{4}$$

where the origin of coordinates is taken to be the center–of–mass of the distribution. In the same fashion, the shape of the charge distribution is characterized by its three principal moments of inertia, which are defined to be the eigenvalues of the moment–of–inertia tensor,

$$\mathbf{I}_{\mu,\nu} = \int d\mathbf{r}\rho^{(2)}(\mathbf{r}) \left(|\mathbf{r}|^2 - r_\mu r_\nu\right) \ , \tag{5}$$

where μ, ν denote Cartesian coordinates and the origin of coordinates is defined at the center of mass, as for Eq. 4; we denote the principal moments of inertia I_1, I_2, and I_3 in descending order. Note that the principal moments of inertia are related to the radius of gyration according to $R_{gyr}^2 = (I_1 + I_2 + I_3)/2$. As a measure of how spherical the distribution is, we also form a symmetry order parameter, η,[24]

$$\eta = \frac{2I_1 - (I_2 + I_3)}{2I_1 + I_2 + I_3} \ , \tag{6}$$

which is zero for spherical distributions and one for an infinitely thin needle.

We are also interested in calculating the diffusion constant of dielectrons, and particularly in comparing the diffusion constant of dielectrons to that of the (single) hydrated electron. We will calculate the diffusion constant from the mean–squared displacement using the Einstein relation,[18]

$$D \;=\; \lim_{t\to\infty} \left\langle |\mathbf{r}(t) - \mathbf{r}(0)|^2 \right\rangle /6t, \tag{7}$$

where $\mathbf{r}(t)$ denotes the position of the center of mass at time t, and the brackets denote an equilibrium ensemble average.[19] We calculate the diffusion constant from the slope of the least–squares line fit to the mean–squared displacement for times 1 ps $< t <$ 2.5 ps.

III. THE EQUILIBRIUM PROPERTIES OF HYDRATED DIELECTRONS

In this Section, we consider the equilibrium properties of fully–formed dielectrons; we will defer a discussion of their formation and kinetic stability to a subsequent publication. A simple description of the hydrated dielectron begins with the cavity model for the (single) hydrated electron. In this zeroth–order picture, a hydrated electron is considered to occupy an attractive, spherical cavity with the attraction caused by the electronic and nuclear polarization of the surrounding solvent molecules. As pointed out in the Introduction, this simple picture is consistent with both continuum dielectric calculations[3] and more sophisticated discretized path–integral calculations.[5] In addition, mixed quantum/classical calculations, in which the excess electron interacts with the (closed–shell) water molecules through a pseudopotential, have shown that besides the spherically–symmetric cavity–bound ground state, the hydrated electron has three p–like cavity–bound excited states, as well as a higher–lying continuum of delocalized states.[6,7,20] Calculations using the same electron–water pseudopotential that we use here give a ground state energy for the (single) hydrated electron of roughly –2.7 eV, with the three p–like excited states ∼2.5 eV higher in energy.[25] Because the cavity occupied by the electron is not perfectly symmetrical, these p–like excited state are split in energy by ∼0.5 eV.[25]

Given this picture for the hydrated electron, what might we anticipate for hydrated dielectrons? For the singlet dielectron, we anticipate that the ground state primarily will consist of both electrons in the same single–electron (ground) state in a single cavity. [For

now, we will neglect the case of two electrons in widely separated cavities, which we will explore elsewhere.] To reduce the Coulomb and exchange repulsion, the cavity containing the dielectrons ought to be larger than for a single electron, but not so large as to significantly disrupt the hydrogen–bonding network of the surrounding solvent; the actual size of the cavity will depend on the balance struck between lowering the Coulomb and exchange energies and optimizing the solvation structure around the dielectron.

In contrast, for the triplet dielectron the Pauli exclusion principle requires that the electrons never occupy the same single–electron state. We therefore anticipate that the triplet dielectron ground state will consist largely of one electron in the single–electron ground state of the cavity and the other electron in the first excited state. The ground and excited states need not occupy the same spatial regions, so it is quite possible that the triplet dielectron could end up not being confined to a single cavity. We shall see later that the triplet dielectron does occupy a single cavity, but this cavity has two lobes that allow the electrons to avoid each other, as required by the Pauli principle.

The equilibrium average properties of the singlet and triplet dielectron ground states are displayed in Table I, along with the corresponding values for the (single) hydrated electron for comparison. Because the distinct spin states do not mix in the absence of magnetic fields, we will discuss the singlet and triplet results separately.

A. Energetics, geometry, and solvent structure

1. The singlet hydrated dielectron

We first examine the energetics of the singlet–dielectron ground state, which are summarized in Table I. The average ground state energy of the singlet dielectron is about –6.0 eV, including +4.7 eV coming from the electron–electron interaction, demonstrating that the singlet dielectron interacts more strongly with the solvent than does the (single) hydrated electron. We can see this more clearly first by examining the single–electron energies and second by subtracting the electron–electron repulsive energy from the dielctron energy. In the first case, we find that the single–electron ground state energy in the dielectron cavity is –6.0 eV, 3.3 eV lower than for the hydrated electron. This deeper potential well for the dielectron produces 7–8 single–electron cavity–bound states instead of the four bound states

found with the (single) hydrated electron. In the second case, neglecting electron–electron repulsion shows that each electron in the dielectron cavity has an energy of (–6.0 – 4.7)/2 eV = –5.4 eV, fully 2.7 eV lower than the (single) hydrated electron. Although the solvation energies estimated with these two methods differ by 0.6 eV, such a difference is not unexpected because the former analysis neglects the contribution of higher–lying product–basis states to the dielectron ground state.

Why does the solvent cavity around the dielectron produce a deeper well than that around a single electron? Some of the extra stabilization results from the the larger size of the dielectron (see Table I and Fig. 3, below), which decreases the kinetic energy per electron from ∼2.3 eV to ∼1.7 eV. However, this 0.6 eV reduction in kinetic energy still leaves –2.1 eV per electron that must come from more favorable electron–solvent interactions in the case of the dielectron. This extra solvation energy results from the larger radius of gyration of the dielectron (Table I), which allows more water molecules to occupy the first solvation shell. The magnitude of the extra stabilization can be estimated by the following scaling argument. For the (single) hydrated electron, the average electron–solvent interaction energy is approximately –5.0 eV, and we expect that this energy comes predominantly from interactions with molecules in the first solvation shell. For compact charge densities, such as the (single) hydrated electron or singlet dielectron, the number of first–shell molecules should be proportional to R_{gyr}^2 (Table I), and in fact scaling the (single) hydrated electron's solvation energy by the ratio of the squares of the radii of gyration predicts a solvation energy per electron of approximately –7.0 eV for the dielectron. This –2.0 eV enhancement of the solvation energy is in very good agreement with the –2.1 eV found directly from the dielectron simulation.

The scaling argument in the above analysis implicitly assumes that the hydrated electron and dielectron have charge densities with similar (spherical) shapes. However, the moments of inertia for the singlet dielectron, which are are also given in Table I, show that the dielectron charge density is significantly aspherical (this can also be seen in the representative charge density displayed in Fig. 1), with $I_1 \sim I_2 > I_3$. The dielectron can therefore be characterized as a slightly lopsided prolate spheroid (i.e. a potato), with a symmetry parameter (Eq. 6) η=0.14.[30] The distortion of the dielectron away from the more spherical symmetry of the (single) hydrated electron (for which $\eta = 0.06$) is caused by the electron–electron repulsion, which forces the two–electron ground state to include contributions from

several higher–lying product basis states other than $|1,1>_+$. To reduce the energy of these higher–lying states, it becomes favorable for the dielectron to break the spherical symmetry of the cavity. In other words, the electron loses its symmetry due to a kind of Jahn–Teller distortion.[23] The broken spherical symmetry of the singlet dielectron is therefore caused by a combination of two effects: the electron–electron interaction that mixes higher–lying product–states into the two–electron ground state, and the subsequent stabilization of these higher–lying states by Jahn–Teller distortion of the solvent cavity.

We turn next in our study of singlet dielectrons to examining which product–basis states, $|n,m>_+$, dominate the ground state wavefunction, $|\Psi_1>_+ = \sum_{n,m} c_{nm}|n,m>_+$. In the limit that there is no electron–electron repulsion, the ground state dielectron wavefunction would simply have both electrons in their single–electron s–like ground states, $|\Psi_1>_+ = |1,1>_+$, but the electron–electron interaction mixes in higher–lying product states so as to lower the Coulomb and exchange repulsion. We find that for every solvent configuration, the dielectron wavefunction is dominated by state $|1,1>_+$, with $|c_{1,1}|^2 \simeq 0.77$ averaged over all configurations. In addition, there is a considerable contribution from two other configurations: one with both electrons in the first single–electron excited state (which resembles a p orbital, complete with angular node), $|c_{2,2}|^2 \simeq 0.07$, and the other with one electron in the ground state and one in the fourth single–electron excited state (which resembles a d_{z^2} orbital), $|c_{1,5}|^2 \simeq 0.06$. We have examined the charge distributions of the single–electron states for representative solvent configurations and have found that the lobes of the p–like and d–like states that compose these low–lying product basis states tend to be aligned along the long axis of the singlet–dielectron cavity. The remaining 10% of the singlet dielectron wavefunction is divided among roughly 15 other product states, none of which have $|c|^2$ greater than 0.01. To clarify the composition of the singlet dielectron ground state, Fig. 2 shows the charge density contours for the ground ($|1>$, s–like), first excited ($|2>$, p–like), and fourth excited ($|5>$, d–like) *single* electron states for a representative *dielectron* water configuration. The figure also displays the charge densities associated with the three product states, ($|1,1>_+$, $|2,2>_+$ and $|1,5>_+$) that together make up $\simeq$90% of the full dielectron ground state. Although this figure does give a flavor for how the p–like and d–like states help to fill dielectron cavity, it is important to remember that the full two–electron state is a sum of product *wavefunctions*, not charge densities. For example, Fig. 2 shows that both of the product states $|1,5>_+$ and $|2,2>_+$ have lobes lying outside

the charge distribution of the dielectron, but these lobes cancel each other because the two product–basis states enter the CI expansion with opposite phases.

Another important question to consider is to what extent do the electrons that make up the singlet dielectron retain their individual identities? Since the singlet dielectron occupies a single cavity in the solvent, we would not expect to be able to view the two electrons as distinct entities. This is clearly seen in the magnitude of the exchange energy relative to the direct Coulomb repulsion, $\alpha = |V_{ex}/V_c| \simeq 0.8$. Despite the significant overlap between the two electrons, however, the mixing in of higher–lying product states does help them to avoid each other, as evidenced by α being less than 1.0.[27] Geometrically, we can see evidence that the electrons do avoid each other by examining the root–mean–squared separation between the electrons ($r_{12} = \langle\Psi|(\mathbf{r}_1 - \mathbf{r}_2)^2|\Psi\rangle$, see the Appendix), as shown in Table I. At first glance, the large value of $r_{12} = 3.9$ Å appears rather surprising because it suggests that the two electrons conspire to be almost as far apart as they can be given that the size of the cavity is $2R_{gyr} \simeq 4.8$ Å. However, we show in the Appendix that when both electrons occupy the same single–electron ground state, the r_{12} parameter is simply related to the radius of gyration, $r_{12}^2 = 2\ R_{gyr}^2$. Therefore a better way to measure the average separation between the two electrons in a single dielectron cavity is to subtract the contribution from the finite extent of each electron. Thus, we define the *excess* separation, $\Delta r_{12} \equiv \sqrt{r_{12}^2 - 2\ R_{gyr}^2}$, as a measure of how effectively the two electrons in the singlet dielectron cavity avoid each other. The electrons in the singlet hydrated dielectron have an excess separation $\Delta r_{12} = 1.9$ Å, an excess that amounts to nearly 40% of the average cavity diameter. Although the two electrons in the dielectron do avoid each other to a good extent, the appreciable ratio of exchange to Coulomb energies shows that the singlet dielectron really is a two–electron quantum object that cannot accurately be described in terms of distinguishable single electrons. This is highlighted by the fact that ∼23% of the total two electron wavefunction comes from higher–lying product–basis states.

What effect does the single dielectron have on the structure of the surrounding water molecules? Figure 3 displays radial distribution functions (RDF) between the dielectron center–of–mass and the classical solvent sites. We define the first solvation shell as the set of all water molecules whose oxygen site lies inside the first minimum of the oxygen–dielectron RDF at 4.2 Å, and find on average that there are 8.6 molecules in the first shell. This number is approximately what we would expect in light of the success of our earlier scaling

argument in explaining the dielectron solvation energy. The (single) hydrated electron has $\simeq 6$ molecules in its first solvation shell, and scaling this number by the relative surface–areas of the single and dielectron gives $6 \times (2.4/2.0)^2 = 8.4$ first–shell waters. Thus, each first–shell water contributes about equally to the solvation of both single and dielectrons; the dielectron is better solvated simply because it is larger and therefore has more first–shell waters.

The RDFs also show that on average one of the O–H bonds on each first–shell water molecule points toward the dielectron (see also Fig. 1), with a separation between the first hydrogen and oxygen peaks of about 0.94 Å. This result is consistent with the $\sim$ 1–Å separation between the peaks for the (single) hydrated electron, which is solvated by each of its six first–shell water molecules pointing one of their 1.0–Å long O–H bonds directly at the electron (i.e. by hydrogen bonding). The smaller separation between the first peaks for the singlet dielectron likely results from the aspherical shape of the dielectron. The simulations show that the first–shell O–H bonds point towards the local maximum dielectron charge density, which given the asphericity means that they point slightly away from the dielectrons's center–of–mass. The fact that the dielectron has the same sort of hydrogen bonding as the single electron also helps to justify our earlier scaling argument for the solvation energy, which could work only if each first–shell solvent molecule's orientation relative to the dielectron were the same as in the first shell of the single electron — as is evidently the case.

2. The triplet hydrated dielectron

Unlike the spin singlet case, when the electron spins are triplet paired it is impossible for both electrons to occupy the same single–electron eigenstate. We would therefore expect the product–basis state that contributes the most to the triplet dielectron wavefunction to have one electron in the single–electron ground state and the other in the first excited single–electron state, $|1,2>_-$, and we find that this is indeed the case. Our calculations show that on average the triplet dielectron wavefunction has $|c_{1,2}|^2 \sim 0.9$. Only three other product states contribute more than 1% to the total: $|2,3>_-$, with $|c_{2,3}|^2 \sim 0.03$; $|2,4>_-$, with $|c_{2,4}|^2 \sim 0.03$; and $|2,5>_-$, with $|c_{2,5}|^2 \sim 0.02$. The triplet dielectron therefore shows much more of a single–configuration character than the singlet dielectron, presumably because

the exclusion of the $|1,1>$ product state reduces the Coulomb repulsion that mixes in the higher–energy product configurations.

The ground–state energy of the spin–triplet dielectron, given in Table I, is –4.7 eV, including +3.1 eV from the Coulomb and exchange energies. As was the case for the singlet dielectron, the electrons that make up the triplet dielectron see a deeper solvent well than in the (single) hydrated electron case, with a single–electron ground–state energy of ∼–4.8 eV. This deeper well produces between six and seven bound single–electron states instead of the four that are typical of (single) hydrated electrons. Unlike the singlet dielectron, however, the single–electron energies of the triplet dielectron do not show a spacing distribution typical of a spherically–symmetric cavity. Instead of the single low–lying state separated from three p–like states and higher–lying d–like states that we saw for the case of the singlet dielectron, the triplet dielectron's cavity produces two low–lying states, at energies of –4.8 eV and –3.3 eV, separated from a band of higher lying states whose energies are all within 0.5 eV of their neighbors. This pattern suggests that the triplet dielectron is far less spherical than the singlet dielectron, and the sphericity paramter, $\eta \sim 0.2$ (see Table I), shows this to be the case. Table I also shows that the triplet dielectron possesses a definite *cylindrical* symmetry, as indicated by the equality of the two largest moments of inertia. For such an aspherical distribution, the radius of gyration is not very meaningful, but we include it in Table I for completeness; gyration parameters describing the principal axes of the triplet dielectron can be obtained from the principal moments of inertia given in Table I. The cylindrical symmetry of the triplet dielectron can be seen in the charge density shown in Fig. 1: the triplet dielectron has a peanut shape, with the distance between the two lobes being a bit over 5 Å; see Fig. 1.

A similar peanut shape also has been seen in the spin density functional calculations of Kaukonen *et al.* for two electrons in a water cluster.[24] In their simulations, Kaukonen *et al.* ran classical dynamical trajectories but took both the oxygen and hydrogen masses to be 1 *amu*, so that the trajectories served to sample configurations rather than to produce true dynamics. Their calculation always took the two–electron density to be that of the lowest energy state, and found that the ground state dielectron charge density switched between two distinct shapes, a "compact" nearly spherical one and an aspherical "dumbbell." We believe that the abrupt shape changes in Kaukonen *et al.*'s calculation arise from the lack of spin coherence in the spin density functional method, which allows fictitious intersystem

crossings in the "dynamics" because the ground state can have either singlet or triplet spin character. Indeed, the spin polarizations reported by Kaukonen *et al.* give a net spin of zero for the "compact" dielectron and a nonzero spin polarization for the "dumbbell." We therefore identify their "compact" and "dumbbell" states as singlet and triplet dielectrons, respectively.[28] We see no such intersystem crossings because our simulations neglect magnetic fields and thus enforce spin coherence at all times. The fact that spin flips were observed in Kaukonen *et al.*'s spin–incoherent simulations, however, shows that occasionally the singlet and triplet dielectron energy levels can cross, suggesting that even weak magnetic fields may induce spin mixing and intersystem crossings. We will explore the importance of magnetic fields and their ability to induce spin flips in a subsequent publication.

For the triplet dielectron, the average electron–electron separation $r_{12} = 5.4$ Å, but as we discussed for the singlet case and show in the Appendix, the value of r_{12} is determined not just by how much the electrons avoid each other but also by the dispersion of the single–electron wavefunctions. As we have pointed out, the triplet dielectron is composed largely of a symmetrized product of the lowest two single electron states, $|c_{1,2}|^2 = 0.89$, and each of these two states has amplitude in both lobes of the "peanut," giving rise to a nonzero exchange energy. Unlike the singlet case, however, the overlap between these two single–electron states is not complete, so it is not clear how to construct an excess separation parameter, Δr_{12}, for the triplet dielectron. We can show that the electrons do avoid each other, however, from the ratio of exchange to Coulomb energies, $\alpha = |V_{ex}/V_c| \simeq 0.3$ (Table I). The small value of α shows that we can roughly consider one electron to be in each lobe of the peanut, with only slight overlap between the two individual electrons.

Let us now turn from the energy and shape of the triplet dielectron to study how the solvent packs around this peanut–shaped object. Because the charge distribution of the triplet dielectron is more cylindrically than spherically symmetric, the solvation structure around the triplet dielectron cannot be readily described in terms of *radial* distribution functions, and must instead be described by a cylindrical distribution function,[7]

$$g_{cyl}(\rho_{cyl}, z)\ d\rho_{cyl}\ dz = \frac{1}{2\pi\rho_{cyl} n} N(\mathbf{r}) d\mathbf{r}\ , \tag{8}$$

where the origin is at the center of mass of the dielectron, $N(\mathbf{r})d\mathbf{r}$ is the number of solvent sites within a small volume $d\mathbf{r} = \rho_{cyl} d\rho_{cyl} d\phi dz$ of the position $\mathbf{r}$, the z–axis is taken to be parallel to the principal axis of the smallest moment of inertia (the long axis of the

peanut), ρ_{cyl} is the distance from this axis, and n is the number density of solvent sites. The distribution averages over the azimuthal angle about the z–axis and because of the symmetry of the charge density, we calculate g_{cyl} by also averaging over both the $+z$ and $-z$ bins.

The upper and middle panels of Fig. 4 show the cylindrical distribution functions of hydrogen atoms and oxygen atoms, respectively, while the bottom panel shows a 2:1 weighted sum of the hydrogen and oxygen distributions. The upper two panels reveal that the triplet dielectron excludes the water from the peanut–shaped cavity occupied by the electrons. The most pronounced solvent structure is located in the "neck" of the dielectron, where we see that an oxygen atom tends to lie midway between the two lobes about 2.3 Å off of the long axis. The figure also shows two hydrogen peaks between the oxygen and each lobe of the triplet dielectron that are roughly 1 Å from the oxygen atom. However, only one of these hydrogen peaks results from the same water molecule as the central oxygen atom — the other peak is an artifact of the cylindrical symmetry. Thus, this pattern of the O and H peaks in the distributions tells us that for waters in the neck region, one O–H bond points directly toward the maximum charge density in one lobe of the dielectron, while the other O–H bond is less strongly constrained by the dielectron and rotates freely to make favorable H–bond interactions with water molecules in the second shell. This rotational freedom, which can also be seen in the breadth of the second peak of the hydrogen $g(r)$ for the case of the singlet dielectron, explains why no sharp peak associated with the "un–bonded" H atom appears in g_{cyl}. The second O–H bond of the water whose oxygen is in the neck region of the triplet dielectron can be distinguished, however, in the bottom panel of the Fig. 4, as the upper lobes of the butterfly–shaped wings surrounding the large oxygen peak. We have counted the average number of oxygen atoms that reside in the neck region -1.0 Å $\leq z \leq 1.0$ Å and $\rho \leq 3.0$ Å; we find that 50% of the triplet dielectron configurations have two oxygen atoms in the neck region, 25% have three, 20% have just one and the remaining configurations have either zero or four molecules in the neck.

Outside the neck region, there is little obvious molecular structure, but by analyzing the isodensity contours we find strong evidence for H–bonding of the first–shell water molecules to the triplet dielectron. In particular, the distance between the $g_{cyl} = 0.8$ contour for hydrogen (shown as the white line in the middle panel of Fig. 4) and the $g_{cyl} = 0.8$ contour for oxygen is roughly 1 Å when measured along a line between the center of the nearest lobe and

the point in question. This tells us that the triplet dielectron's first solvation shell consists of water molecules whose O–H bonds point radially towards the nearest maximum charge density. Therefore, just as for the (single) hydrated electron and for the singlet dielectron, the water structure around the triplet dielectron consists of local hydrogen bonding, which allows the first–shell waters to both solvate the charge and to maintain hydrogen bonding to outer–shell waters.

B. Dynamical Properties of Hydrated Dielectrons

In this Section, we analyze the dynamical properties of dielectrons by forming normalized autocorrelation functions of dielectron energetic and structural properties,

$$C_A(t) \;=\; \frac{\langle \delta A(t) \delta A(0) \rangle}{\langle \delta A(0)^2 \rangle} \;, \tag{9}$$

where $\delta A = A - < A >$, and A is the property of interest, t the time, and the angled brackets denote an equilibrium average. The correlation functions we display in this Section were generated from the 30–ps equilibrium runs described in Section II. Figures 5 and 6 show the full dynamical histories of several properties of the singlet and triplet dielectron, respectively. Although we will not discuss the individual trajectories in detail, we do note that the adiabatic energies and geometrical properties of dielectrons vary rapidly on timescales associated with individual water vibrations and librations. The Coulomb and exchange energies, in contrast, do not show the fast wiggles that are indicative of strong modulation by individual water molecules. It is noteworthy that twice during the 30 ps triplet dielectron trajectory the root–mean–squared separation, r_{12}, increased rapidly (bottom panel, Fig. 6) before returning to its equilibrium value. Thus, it seems that the triplet dielectron made two failed attempts to dissociate in just a few tens of picoseconds.

1. Dynamics of the hydrated singlet dielectron

Figure 7 shows the autocorrelation functions of the singlet dielectron ground–state energy, ground–to–first–excited–state energy gap, Coulomb energy, and exchange energy (*cf.* Fig. 5). Clearly, both the ground state energy and the ground–to–first–excited–state energy gap decorrelate rapidly, on the timescale of the intramolecular motions of water. The power

spectra of these two correlation functions (not shown) show that the initial "bounce" at $t = 20$ fs and subsequent ringing features arise from the coupling of the dielectron energies to water bends and stretches, whereas the slower decay results from librations and translations. The rapid oscillations in the energy gap are much smaller in amplitude than those for the ground state energy because water motions that rapidly modulate the ground state tend to likewise modulate the excited states, so that the *gap* varies less than the individual energy levels (*cf.* Fig. 5). This difference in the rate at which the energy levels and energy gaps decorrelate is similar to that seen with the single hydrated electron.[6,7]

In contrast to the full quantum energies, the autocorrelations of the Coulomb and exchange energies display very little ringing and decay more slowly, meaning that the Coulomb and exchange energies are only weakly affected by the intramolecular motions of nearby water molecules. This is not surprising because even though the electron–water pseudopotential is short–ranged, most of the electron–electron interaction energy comes from regions of high electron density, near the center of the dielectron cavity. Because high–density regions are always far from the water molecules, intramolecular vibrations have little effect on the "core" of the dielectron charge density. Slower motions are able to couple to the Coulomb and exchange energies, however, because large–scale librations and translations can gradually change the entire shape of the electron density and hence alter the electron–electron interactions.

Figure 8 displays the autocorrelation of three measures of the dielectron geometry: the radius of gyration, R_{gyr} (Eq. 4), the quantum separation parameter, r_{12} (Eq. A2), and the symmetry order parameter, η (Eq. 6). All of these geometric measures have autocorrelation functions that closely resemble the Coulomb and exchange energy autocorrelation functions in Fig. 7. This resemblance is to be expected because these geometric measures are all "bulk" quantities in the sense that they depend on integrals over the full charge distribution, so they ought to display similar correlation behavior as the electron–electron interactions. The fact that the quantum separation parameter, r_{12}, also tracks this bulk behavior at first may seem surprising, until one recalls that (for the singlet dielectron) r_{12} is really a measure of the radius of gyration, as discussed in the Appendix.

The final aspect of the dynamics of singlet dielectrons that we shall address is their long–time, diffusive motion: our calculated diffusion constant for the singlet dielectron is given in Table I. The singlet dielectron diffuses more slowly than the (single) hy-

drated electron, which is not all that surprising in view of the dielectron's larger size. According to the Stokes–Einstein relationship, however, the diffusion constant should be inversely proportional to an object's radius. Thus, if the diffusion of these solvent–supported species follows hydrodynamics, the diffusion constant of the singlet dielectron should be related to that of the single electron by a factor of $(2.4/2.0)^{-1}$, which would give $D_{singlet}^{hydro} \simeq 1.7 \times 10^{-5} cm^2/s$. Thus, the diffusion constant of the singlet dielectron calculated in our simulations, $D_{singlet} \simeq 1.9 \times 10^{-5} cm^2/s$, is larger than what would be expected on purely hydrodynamic grounds.

2. Dynamics of the hydrated triplet dielectron

Figure 9 shows the autocorrelations of the triplet dielectron ground–state energy, ground–to–first–excited–state energy gap, Coulomb energy, and exchange energy (*cf.* Fig. 6). As with the singlet dielctron, the ground state energy decorrelates rapidly and shows the ringing that results from coupling to the water bends and stretches. Also as with the (single) hydrated electron and singlet dielectron, the energy gap of the triplet dielectron decorrelates much more slowly than the total energy, because the water bends and stretches tend to modulate all of the energies the same way. The Coulomb energy of the triplet dielectron also decorrelates similarly to that of the singlet dielectron, although the initial rapid decay is slightly greater for the triplet. Interestingly, and unlike the singlet case, the exchange energy of the triplet dielectron decorrelates much more rapidly than the Coulomb energy, and on a timescale consistent with strong coupling to the intramolecular water motions. In fact, the power spectra of the triplet Coulomb and exchange energies (not displayed) show that the water bend and stretch peaks modulate the exchange energy 2–3 times more than the Coulomb energy. The stronger modulation of the exchange energy likely happens because the exchange energy depends on the overlap between the product–basis wavefunctions that could be strongly affected by water motions in the "neck" of the triplet dielectron. Such motions would have little effect on the triplet Coulomb energy, which depends only on the overall density and not on the overlap.

Figure 10 displays autocorrelation functions of several measures of the triplet dielectron geometry: the radius of gyration, R_{gyr} (Eq. 4), the quantum separation parameter, r_{12} (Eq. A2), and the symmetry order parameter, η (Eq. 6). Each correlation function decays rapidly,

followed by a slower falloff, just as we saw for the Coulomb and energy gap correlation functions, however the amplitude of the initial fast decay (20–25%) is smaller for these geometric quantities than for the energy decays (30–35%). The smaller amplitude of the rapid decay is consistent with the idea that these geometric measures of the dielectron geometry depend mostly on gross features of the dielectron's shape that are modulated only by collective (and hence slow) water motions.

One other geometric property whose dynamics is of interest is the orientation of the triplet dielectron. We define the orientation vector, $\hat{\mathbf{\Omega}}_{\mathbf{3}}$, to be the unit vector pointing in the direction of the smallest principle moment of inertia (i.e. $\hat{\mathbf{\Omega}}_{\mathbf{3}}$ points along the long axis of the dielectron). During the 30 ps of our equilibrium run, the triplet dielectron orientation vector does not decorrelate, and the correlation function never dips below 1/2.[31,32] This result is not all that surprising if we envision the peanut as a classical object: it is well known that molecules of roughly the same size as the triplet dielectron take tens to hundreds of picoseconds to rotationally decorrelate in water.[33] Apparently, the extra freedom to wiggle that quantum mechanics allows for the solvent–supported triplet dielectron does not help it to rotate any better than a classical object of similar size.

We conclude our discussion of dynamics of the triplet dielectron by examining its long–time, diffusive motions. The diffusion constant, given in Table I, shows that the triplet dielectron diffuses significantly more slowly than either the singlet dielectron or the hydrated electron. This is not surprising given the large size and highly non–spherical shape of the triplet dielectron. Is this difference due solely to geometry? To make the hydrodynamic calculation straightforward, we can crudely model the triplet charge distribution as a prolate spheroid. For a prolate spheroid with semiaxes $a = 2.5$ Å and $c = 5.8$ Å,[34] the diffusion constant, D, is related to that of a sphere of radius r by a factor $(2r/3c + r/3a)$, which would give $D^{hydro}_{triplet} = 1.0 \times 10^{-5} cm^2/s$ when scaled to the (single) hydrated electron's diffusion constant. The triplet dielectron therefore diffuses faster than would be predicted on purely hydrodynamic grounds as we also saw for the singlet dielectron. On the other hand, scaling the singlet dielectron's diffusion constant by the factor $(2R_{gyr}/3c + R_{gyr}/3a)$, with R_{gyr} the singlet–dielectron radius of gyration, gives a predicted triplet diffusion constant $D^{hydro}_{triplet} \simeq 1.1 \times 10^{-5} cm^2/s$, which is within the error of the simulated value. It seems therefore that we can consider dielectrons in either spin state to move in a solvent whose effective viscosity is roughly 20% smaller than the effective viscosity around the single electron.

IV. EXPERIMENTAL SIGNATURES OF DIELECTRONS: OPTICAL ABSORPTION OF THE SINGLET AND TRIPLET HYDRATED DIELECTRON

Now that we have some insight into the basic properties and dynamics of dielectrons, it is natural to ask how one might experimentally observe this species. Because the CI method produces accurate excited states as well as the ground state, we can compute quantities such as absorption spectra and thus predict experiments to directly observe these two–electron species. We should point out that the model we are using for the electron–water pseudopotential is known to produce an absorption spectrum of the (single) hydrated electron that is shifted to the blue of the experimentally measured spectrum by roughly 0.7 eV.[25] Other models recently have been introduced that correct this problem by altering the pseudopotential or adding polarizability to the water.[20,35] However, our choice of the Schnitker/Rossky pseudopotential allows us to make detailed comparisons of the spectra of single electrons and dielectrons using the best–characterized single–electron model.[6,25]

We compute the absorption spectrum of dielectrons in their ground states (denoted state 1) in the inhomogeneous broadening limit,

$$\sigma^{\pm}(E) \;=\; \frac{4\pi^2\hbar^2}{m^2E}\left(\frac{e^2}{\hbar c}\right)\sum_{j=1}^{N}|\;{}_{\pm}<\Psi_j|\hat{\epsilon}\cdot\mathbf{P}|\Psi_1>_{\pm}|^2\delta(E_j-E_1-E), \tag{10}$$

where E_i is the energy of the i–th two–electron adiabatic eigenstate, $\hat{\epsilon}$ is the polarization vector of the incident radiation and $\mathbf{P} = \mathbf{p}_1 + \mathbf{p}_2$ is the two–electron momentum vector operator, and the subscripts refer to which electron each operator acts upon. For the two–electron wavefunctions, $|\Psi_i>_{\pm}$, the plus sign subscript denotes the spin singlet case and the minus sign subscript is used for the spin triplet case. In calculating the spectra we have made use of the selection rule that dipole transitions do not flip spins, so that states are only coupled from the same spin manifold. In practice, we take advantage of the CI form of our wavefunctions to write Eq. 10 as a linear combination of matrix elements connecting the single–electron product states,

$${}_{\pm}<\Psi_j|\hat{\epsilon}\cdot\mathbf{P}|\Psi_1>_{\pm}=\sum_{n'm'}\sum_{nm}(c^j_{n'm'})^*c^1_{nm}\;{}_{\pm}<n'm'|\hat{\epsilon}\cdot(\mathbf{p}_1+\mathbf{p}_2)|nm>_{\pm}, \tag{11}$$

where the product states $|nm>_{\pm}$ are defined in Eq. 2.[36] Equation 2 shows that writing the dielectron wavefunctions in terms of the single–electron product states, $|nm>_{\pm}$, gives terms in the absorption spectrum proportional to the square of ${}_{\pm}<n'm'|\mathbf{p}_1+\mathbf{p}_2|nm>_{\pm}$.

If the product wavefunctions are expanded, it is clear that the transition dipoles between product states vanish unless one of the following conditions holds: $n' = n$, $n' = m$, $m' = n$, or $m' = m$. Schematically, then, we can say that the allowed electric dipole transitions for dielectrons excite only one of the electrons at a time. [Note that this statement would literally be true if the dielectron state consisted solely of a single product–basis state.]

As noted in Section II, we construct the two–electron eigenstates using the lowest 10 single–electron states, so that N in Eq. 10 is 55 and 45 for singlet and triplet dielectrons, respectively. To test the accuracy of using this number of single–electron states for our product basis, we also have computed the oscillator strength for the (single) hydrated electron and both dielectrons, which is proportional to $\int d\omega\ \omega\ \sigma(\omega)$. According to the Thomas–Reich–Kuhn sum rule,[37] the oscillator strength of the dielectron absorption should be exactly twice that for a single electron. With 10 single–electron states used to construct the two–electron basis, we find singlet and triplet dielectron oscillator strengths that are 1.72 and 1.86 times larger than for a single hydrated electron, respectively. This indicates that use of only the lowest 10 single–electron states does not generate a two–electron product basis that is complete enough to rigorously satisfy the sum rule. We have run test calculations of the oscillator strength as a function of the number of single–electron basis states used to construct the CI wavefunctions for one singlet and one triplet dielectron configuration, with the results shown in Table II. As the number of single–electron states is increased, the total oscillator strength indeed approaches 2.

Figure 11 shows the absorption spectra of both singlet and triplet dielectrons, as well as the absorption spectrum of the (single) hydrated electron for this model. The spectra of both singlet and triplet dielectrons overlap with the single hydrated electron absorption, but both types of dielectrons also display significant absorption to the *blue* of the single electron. The "extra" dielectron absorption at high frequencies results from two effects. First, we saw in Section III A that both singlet and triplet dielectrons occupy solvent cavities with much deeper attractive wells for the resident electrons. This lowers the ground–state single–electron energies and also pulls additional bound single–electron states down from the continuum, giving rise to the blue tail in the absorption. Second, both the singlet and especially the triplet dielectron's solvent cavities are more asymmetrical than the single electron's, which leads to a greater energy splitting between the lowest dielectron excited states than between the three p–like single–electron states, producing a broader absorption

spectrum.

Do these calculated spectra shed any light on the question of whether dielectrons have been observed? A variety of indirect experiments are consistent with the existence of dielectrons. For example, the magnetic susceptibility of electrons dissolved in liquid NH_3 is found to decrease as the density of electrons increases, suggesting that at high enough electron densities, the electrons begin to form singlet pairs;[38] such (peanut–shaped) singlet pairs were observed in the DFT calculations of Klein and coworkers.[13] In addition, Schmidt and Bartels examined how the $e^- + e^-$ annihilation rate varies with ionic strength in solutions of electrons in water and concluded that the measured rate requires the formation of an intermediate species, which is presumably the spin–singlet dielectron.[39] While the aforementioned results are consistent with the existence of dielectrons in solution, our results suggest that the most straightforward way to directly observe dielectrons is to look for a concentration dependence of the absorption in the blue tail of the (single) hydrated electron's spectrum. Although such an excess has not been observed directly, Walker and coworkers found that highly basic solutions of hydrated electrons at high concentrations absorbed light to the blue of the single–electron spectrum, and that this absorption led to a transient increase in absorption at the peak of the hydrated electron spectrum.[40] Their conclusion was that whatever was absorbing the blue light produced additional hydrated electrons, and they tentatively identified the species as dielectrons (which were photodissociated to produce (single) electrons). This identification has been challenged by Meisel *et al.*, who concluded from pulse radiolysis measurements that if the dielectron exists, either it does not absorb light in the ultraviolet or it is much shorter–lived than (single) hydrated electrons under the same conditions.[41] Telser and Shindewolf have also disputed Walker *et al.*'s interpretation, and they have identified the blue–absorbing intermediate species as a solvated neutral metal atom.[42] Our computed spectra are consistent with the observations of Walker *et al.*, but a complete test of the photodissociation scenario will require nonadiabatic simulations of photoexcited dielectrons. Such a non–equilibrium calculation is beyond the scope of this paper, but the calculations are in progress and will be presented soon.

V. DISCUSSION

In this paper, we have focused on the equilibrium properties of hydrated dielectrons, which are an example of perhaps the simplest possible solvent–supported, multi–electron quantum object. By using full CI to solve the two–electron quantum part of the problem, we have been able to include the effects of exchange, correlation, and spin statistics *exactly*; CI also generated the excited states needed to compute the absorption spectrum of these species.

Our calculations show that exchange and spin statistics have a significant effect on both the energetics and geometry of dielectrons. The mobility of solvent molecules acts in concert with the ability of electronic wavefunctions to change shape so that singlet and triplet states of the dielectron have very different shapes, energies, and absorption spectra. The differences between the two types of dielectron can be rationalized rather easily by invoking a simple version of the Pauli exclusion principle: triplet–paired electrons avoid each other more than singlet–paired electrons do. Of course, the particular shape of each type of dielectron depends on striking a balance between lowering the electron–electron repulsion and minimizing the disruption to the solvent structure, leading to qualitatively different equilibrium shapes for singlet and triplet dielectrons. Interestingly, for both singlet and triplet dielectrons, this balance always works to maintain optimal hydrogen bonding of the water molecules to the charge density.

Unlike the equilibrium shapes and energies, the dynamics of most dielectron properties are not all that different from the dynamics of the (single) hydrated electron. Most quantities showed decorrelation on multiple timescales, indicating coupling to both intramolecular and intermolecular solvent motions, just as was seen for the (single) hydrated electron. The only quantities whose dynamics differed qualitatively from the single electron dynamics were the electron–electron interactions, which showed very little coupling to rapid, intramolecular water motions — just as would be expected for diffuse distributions of charge that are only changed at their edges by rapid water motions. The basic similarity of the dielectron and single–electron dynamics suggests that both species behave about the same as far as the solvent is concerned, as we would expect in view of the similar hydrogen–bonded solvation structures: the solvent simply sees an amorphous blob of charge (albeit with slightly different sizes and shapes) and moves in roughly the same way regardless of whether there are one or

two electrons.

Finally, it is worth noting reiterating that we have not allowed any mixing between singlet and triplet states because such mixing can occur only in the presence of magnetic fields. Liquid water does possess moving charges and hence locally fluctuating magnetic fields, so nuclear motions of the solvent could conceivably induce intersystem crossings — particularly when the singlet and triplet dielectron energy levels cross. We pointed out above that such intersystem crossings did occur in Kaukonen *et al.'s* density functional simulations (although this was an artifact of their simulation method), telling us that the lowest singlet and triplet dielectron energy levels do occasionally cross. This suggests that even weak coupling between the singlet and triplet spin manifolds could induce spin mixing and intersystem crossings. The possibility of intersystem crossing suggests also that internal conversion of excited singlet dielectrons could produce long–lived triplet dielectrons. Indeed, because the absorption spectrum of the triplet dielectron overlaps significantly with that of the (single) hydrated electron, the experiments that Walker and coworkers[40] interpreted as the photodissociation of singlet dielectrons to form (single) hydrated electrons are also consistent with the formation of long–lived triplet dielectrons following crossing of an excited dielectron from the singlet to the triplet manifold. This sort of internal conversion could also be important in the photophysics of charge transfer processes, such as charge–transfer–to–solvent (CTTS) reactions,[43] because any internal conversion of an excited–state electron could prevent recombination of the excited state, and thus could have a significant effect on CTTS dynamics. Our CI algorithm can be extended to include such mixing between spin manifolds for multiple electrons at essentially no additional computational cost, but we leave these interesting issues to future work.

Acknowledgments

We are pleased to acknowledge helpful discussions with Jay Smallwood and Michael J. Bedard–Hearn. We also thank David M. Bartels for making us aware of Ref. 42 and for his critical reading of the manuscript. The charge densities shown in Fig. 1 were produced using the UCSF Chimera package from the Computer Graphics Laboratory, University of California, San Francisco (supported by NIH P41 RR-01081).[44] This work was supported by the NSF under Grant No. CHE–0204776 and the UCLA Council on Research. B.J.S is

a Cottrell Scholar of Research Corporation and a Camille Dreyfus Teacher–Scholar.

APPENDIX A: QUANTUM–MECHANICAL MEASURE OF THE ELECTRON–ELECTRON SEPARATION

In this Appendix, we explore in detail the properties of our measure of the distance between electrons, r_{12}. We begin by noting that because the electrons are indistinguishable the difference between the average positions of the two electrons in a state $\Psi(\mathbf{r}_1, \mathbf{r}_2)$ vanishes,

$$ {}_{\pm}\langle\Psi|\,\hat{\mathbf{r}}_1 - \hat{\mathbf{r}}_{\mathbf{2}}\,|\Psi\rangle_{\pm} \;=\; 0 \;, \tag{A1} $$

where the bold–faced quantities are vectors, the carets denote quantum mechanical operators, and the subscripts indicate which electron they operate on. Thus, we must come up with some other measure of the distance between two indistinguishable electrons. The simplest such measure of the inter–electron separation is the mean–squared separation, which we define to be

$$ r_{12}^2 \;=\; {}_{\pm}\langle\Psi|\,(\hat{\mathbf{r}}_1 - \hat{\mathbf{r}}_{\mathbf{2}})^2\,|\Psi\rangle_{\pm}\,, \tag{A2} $$

for any normalized two–electron state $|\Psi\ >$. We refer to r_{12} as the *root–mean–squared separation.*

Does this definition give sensible results? Consider, by way of example, the case of two widely separated cavities called the left (L) and right (R) cavities, which have single solvated–electron ground states, ψ_L and ψ_R, respectively. For well–separated cavities the interaction between electrons will be small, so the ground state of the two–electron system can be considered to be a product state with a single electron in the ground state of each hole, $\Psi_0^{\pm} \;=\; (\psi_L(\mathbf{r}_1)\psi_R(\mathbf{r}_2) \pm \psi_R(\mathbf{r}_1)\psi_L(\mathbf{r}_2))/\sqrt{2}$, where the plus sign is for the spin–singlet case and the minus sign is for the spin triplet case. While it is true that each electron occupies *both* cavities, the form of Ψ_0 given above tells us that when one electron is in cavity L, the other must be in cavity R (and vice versa) — thus the two electrons are "separated" from each other. Suppose that the centers of the left and right cavities are separated by a distance d_{LR}, that the single–electron state associated with one cavity has no amplitude to be in the other cavity, and that the single–electron radii of gyration are a_L and a_R, respectively. Then the mean–squared separation between the two electrons is $r_{12}^2 = d_{LR}^2 + (a_L^2 + a_R^2)$, and we see

that the root–mean–squared separation, r_{12}, does give a measure of the distance between electrons in well–separated solvent cavities. Note that if the two cavities merge into a single cavity (and electron–electron interactions are neglected), $r_{12} = a_L\sqrt{2} = a_R\sqrt{2}$.

Although r_{12} is not literally the distance between the two electrons even for electrons confined to a single cavity, the root–mean–squared separation is still a physically meaningful quantity. To see this, we examine the relationship between the electron–electron interaction energy and r_{12}. We expect that if r_{12} is realistic measure of the interelectron separation, the interaction energy should vary approximately as $1/r_{12}$. To quantify this, we have used the 30–ps equilibrium runs to calculate the Spearman rank correlation coefficients of V_c, V_{ex}, and $V_c + V_{ex}$ with $1/r_{12}$ for both singlet and triplet dielectrons; scatter plots of these interactions vs. $1/r_{12}$ are shown in Fig. A1. For the singlet dielectron, the correlation coefficients are 0.811, 0.486, and 0.662, for V_c, V_{ex}, and $V_c + V_{ex}$, respectively. This tells us that for the singlet dielectron, the overlap between the electrons produces an energy that correlates well with a classical, Coulombic point–charge interaction, but that the exchange energy cannot be considered in classical terms. For the triplet dielectron, the correlation coefficients are 0.855, 0.085 and 0.997, for V_c, V_{ex}, and $V_c + V_{ex}$, respectively. The strong correlation between the total electron–electron interaction energy and $1/r_{12}$ suggests that for the triplet dielectron the exchange energy cancels those parts of the Coulomb energy that come from overlap between the single–electron wavefunctions in the "neck" of the triplet dielectron, so that the net interaction goes very nearly as $1/r_{12}$.

---

[1] Marcus, R. A. *J. Chem. Phys.* **1956**, *24*, 966; *Annu. Rev. Phys. Chem.* **1964**, *15*, 155.

[2] Chandler, D; Leung, K. *Ann. Rev. Phys. Chem.* **1994**, *45*, 557.

[3] Jortner, J. *Mol. Phys.* **1962**, *5*, 257; *J. Chem. Phys.* **1959**, *30*, 839. Blandamer, M. J.; Catterall, R.; Shields, L.; Symons, M. C. R. *J. Chem. Soc.* **1964**, 4357. Blandamer, M. J.; Shields, L.; Symons, M. C. R. *J. Chem. Soc.* **1965**, 3759.

[4] Coker, D. F.; Berne, B. J.; Thirumalai, D. *J. Chem. Phys.* **1987**, *86*, 5689;

[5] The path–integral method for solvated electrons is reviewed by Chandler and Leung (Ref. 2. Explicit path–integral calculations for the hydrated electron may be found in Wallqavist, A; Thirumalai, D.; Berne, B. J. *J. Chem. Phys.* **1987**, *86*, 6404 and Laria, D.; Wu. D.; Chandler,

D. *ibid.* **1991**, *95*, 4444, and references contained therein.

[6] Schwartz, B. J.; Rossky, P. J. *J. Phys. Chem.* **1994**, *98*, 4489; **1995**, *99*, 2953; *J. Chem. Phys.* **1994**, *101*, 6917; *Phys. Rev. Lett.* **1994**, *72*, 3282; *J. Mol. Liq.* **1995**, *65–6*, 23. Schwartz, B. J.; Bittner, E. R.; Prezhdo, O. V.; Rossky, P. J. *J. Chem. Phys.* **1996**, *104*, 5942. Wong, K. F.; Rossky, P. J. *J. Phys. Chem. A* **2001** *105*, 2546; *J. Chem. Phys.* **2002**, *116*, 8418; **2002**, *116*, 8429.

[7] Schwartz, B. J.; Rossky, P. J. *J. Chem. Phys.* **1994**, *101*, 6902.

[8] E. Neria, A. Nitzan, R. N. Barnett, and U. Landman, Phys. Rev. Lett. **67**, 1011 (1991).

[9] See *e.g.* Hart, E. J.; Anbar, M. *The Hydrated Electron*; Wiley: New York, 1970, or Bladamer *et al.* in Ref. 3.

[10] Mizuno, M; Tahara, T. *J. Phys. Chem. A* **2001**, *105*, 8823; *ibid.* **2003**, *107*, 2411. Tauber, M. J.; Mathies, R. A. *J. Phys. Chem. A* **2001**, *105*, 10952; *Chem. Phys. Lett.* **2002**, *354*, 2002; *J. Am. Chem. Soc.* **2003**, *125*, 1394.

[11] Bradforth, S. E.; Jungwirth, P *J. Phys. Chem. A* **2002**, *106*, 1286.

[12] A notable exception is the study of the band structure of electrons in a liquid which treated electron–electron interactions at the level of Hartree–Fock theory, Kavanaugh, T.; Stratt, R. M. *J. Chem. Phys.* **1994**, *100*, 3028.

[13] Deng Z. H.; Martyna, G. J.; Klein, M. L. *Phys. Rev. Lett.* **1992**, *68*, 2496; **1993**, *71*, 267; *J. Chem. Phys.* **1994**, *100*, 7590. Martyna, G. J.; Deng, Z. H.; Klein, M. L. *J. Chem. Phys.* **1993**, *98*, 555.

[14] Selloni, A.; Car, R.; Parrinello, M; Carnevali, P. *J. Phys. Chem.* **1987**, *91*, 4947. Fois, E. S.; Selloni, A.; Parrinello, M.; Car, R. *ibid.* **1988**, *92*, 3268.

[15] Fueki, K. *J. Chem. Phys.* **1969**, *50*, 5381.

[16] Larsen, R. E.; Schwartz, B. J. *J. Chem. Phys.* **2003**, *119*, 7672.

[17] Toukan, K.; Rahman, A. *Phys. Rev. B.* **1985**, *31*, 2643.

[18] Chandler, D. *Introduction to Modern Statistical Mechanics*, Chapter 8; Oxford University Press: New York, 1987.

[19] Our dielectron trajectories were assembled by concatenating several shorter runs, and at the beginning of each of these runs the coordinates were shifted so as to place the dielectron at the center of the simulation box. By keeping track of these shifts we can convert our simulated positions (all of which are inside the box) into global coordinates, and thus calculate the diffusion

constant, D.

[20] Turi, L.; Borgis, D. *J. Chem. Phys.* **2002**, *117*, 6186.

[21] As was discussed in detail in Ref. 16, the approximations made in the CI–with–important–states algorithm lead to a small drift in the total energy of ∼0.1 eV/ps. Although temperature is relatively constant despite this drift, to reduce fluctuations of temperature, we have rescaled the magnitudes (but not the directions) of the classical velocities every 2 ps, so as to maintain a constant average temperature.

[22] Laaksonen, L. *J. Mol. Graph.* **1992**, *10*, 33. Bergman, D. L.; Laaksonen, L.; Laaksonen, A. *J. Mol. Graph. Modell.* **1997**, *15*, 301.

[23] Ashcroft, N. W.; Mermin, N. D *Solid State Physics*, Chapter 31; W. B. Saunders: Fort Worth, 1976, Chapter 31.

[24] Kaukonen, H.–P.; Barnett, R. N.; Landman, U. *J. Chem. Phys.* **1992**, *97*, 1365.

[25] Rossky, P. J.; Schnittker, J. *J. Phys. Chem.* **1988**, *92*, 4277.

[26] Allen, M. P.; Tildesley, D. J. *Computer Simulation of Liquids*; Oxford University Press: London, 1992.

[27] We have defined the Coulomb and exchange energies (Ref. 16) such that if the two–electron state consists of a single product basis state with both electrons in the same single–electron state, α will be one.

[28] The sphericity order parameters, η, reported in Ref. 24 are ~ 0.1 and ~ 0.2 for the "compact" and "dumbbell" dielectrons, respectively. These values compare favorably to the values of our singlet and triplet dielectrons, as reported in Table I.

[29] The standard deviations in Table I were calculated by computing the root–mean–square deviation and dividing by the square root of the number of *independent* samples, which was taken to be the length of the run divided by the decorrelation time of the listed property (typical decorrelation times were ∼0.2–1 ps for dielectrons and $\sim$ 2 ps for the single electron).

[30] The pseudopotential we use produces a much more spherically symmetric single–electron charge density than has been reported in the recent *ab initio* density–functional calculations of Parinello et al., Phys. Rev. Lett. **2003**, *90*, 226403–1. The moments of inertia that they report for their (single) electron correspond to $\eta = 0.27$, which is much larger than we find (Table I). We do note, however, that the density–functional calculations of Kaukonen et al., Ref. 24, used a different electron–water pseudopotential than the one we use, and they report values of η for

the "compact" dielectron very similar to those reported here for the singlet dielectron.

[31] Note that because the principle moment of inertia vector is only defined to within an arbitrary sign, we autocorrelated the orientation vector, $\hat{\mathbf{\Omega}}_3$ after forcing the vector at each time to have the maximum overlap with the vector at the previous time.

[32] The average root–mean–squared fluctuation for the two angles that describe the orientation in spherical coordinates is less than 30 degrees.

[33] See Fleming, G. R. *Chemical Application of Ultrafast Spectroscopy*; Oxford: New York, 1986, Table 6.3.

[34] For a prolate spheroid with semimajor and semiminor axes c and a, respectively, the moments of inertia are $I_1 = I_2 = (a^2 + c^2)/5$ and $I_3 = 2a^2/5$, and the results in Table I imply that $a \simeq 2.5$ Å and $c \simeq 5.8$ Å for this model of the triplet dielectron.

[35] Staib, A.; Borgis, D. *J. Chem. Phys.* **1995**, *103*, 2642.

[36] We also can replace the momentum operators with position operators using the well–known single–electron operator identity, $< m|\mathbf{p}|n >= im\omega_{mn} < m|\mathbf{r}|n >$, where m is the mass of the electron, $\omega_{mn} = (\epsilon_m - \epsilon_n)/\hbar$, and $\epsilon_m,\ \epsilon_n$ are the single–electron eigenenergies involved in the transition.

[37] Sakurai, J. J. *Modern Quantum Mechanics, Revised Edition*; Addison–Wesley: Reading, 1994, Chapt. 5, Section 7.,

[38] Edwards, P. P. *J. Supercond.* **2000**, *13*, 933.

[39] Schmidt, K. J.; Bartels, D. M. *Chem. Phys.* **1995**, *190*, 145.

[40] Basco, N.; Kenney, G. A.; Walker, D. C. *Chem. Commun.* **1969**, 917. Basco, N.; Kenney–Wallace, G. A.; Vidyarthi, S. K.; Walker, D. C. *Can. J. Chem.* **1972**, *50*, 2059.

[41] Meisel, D.; Czapski, G; Matheson, M. S.; Mulac, W. A. *Int. J. Rad. Phys. Chem.* **1975**, *7*, 233.

[42] Telser, Th.; Shindewolf, U. *J. Phys. Chem.* **1986** *90*, 5378.

[43] Blandamer, M. J.; Fox, M. F. *Chem. Rev.* **1970**, *70*, 59.

[44] Huang, C. C.; Couch, G. S.; Pettersen, E. F.; Ferrin, T. E. *Pacific Symposium on Biocomputing* **1996**, 1:724. The Chimera code is freely available on the world wide web at `http://www.cgl.ucsf.edu/chimera`.

	$(e_2^-)_{aq}$ – Singlet	$(e_2^-)_{aq}$ – Triplet	$(e^-)_{aq}$
E (eV)	–5.99 (0.17)	–4.71 (0.22)	–2.74 (0.14)
V_c (eV)	2.57 (0.03)	4.30 (0.08)	—
V_{ex} (eV)	2.08 (0.03)	–1.21 (0.02)	—
$V_{aq}^{(a)}$ (eV)	–82.38 (0.56)	–82.62 (0.60)	–87.06 (0.17)
I_1 (Å^2)$^{(b)}$	4.66 (0.16)	8.12 (0.37)	3.08 (0.21)
I_2 (Å^2)$^{(b)}$	4.07 (0.17)	7.92 (0.37)	2.87 (0.20)
I_3 (Å^2)$^{(b)}$	2.99 (0.14)	2.55 (0.06)	2.52 (0.10)
R_{gyr} (Å)$^{(c)}$	2.42 (0.03)	3.04 (0.06)	2.05 (0.05)
r_{12} (Å)$^{(d)}$	3.91 (0.06)	5.38 (0.12)	—
$\eta^{(e)}$	0.14 (0.01)	0.215 (0.003)	0.060 (0.005)
D ($\times 10^{-5}$ cm^2/s)$^{(f)}$	1.87 [0.08]	1.3 [0.2]	2.0 [0.1]

[a] Total water–water interaction energy for all 200 molecules. A 30 ps simulation with no electron in the box yields $V_{aq} = -88.64(0.17)$.

[b] Principal moments of inertia of the dielectron or electron density, defined as the eigenvalues of the moment–of–inertia tensor, Eq. 5.

[c] Radius of gyration of the electron density, Eq. 4.

[d] Quantum separation parameter, Eq. A2, and described in the Appendix.

[e] Symmetry order parameter, Eq. 6.

[f] Translational diffusion constant, Eq. 7, calculated as discussed in Section II. The linear fits for all three species had $R^2 > 0.997$. The numbers in square brackets give the maximum change to D in either direction that will allow a line to lie within one standard deviation of $< |\mathbf{r}(t) - \mathbf{r}(0)|^2 >$ for all times in the range fitted.

TABLE I: Average properties of the ground state of various aqueous electronic species. The columns labelled singlet and triplet give the properties of the dielectron in that spin manifold. All dielectron quantities were calculated from 30–ps trajectories with the two–electron wavefunction restricted to the ground state, whereas the average properties of the (single) aqueous electron were calculated from a single 60–ps trajectory. The numbers in parentheses represent two standard deviations, calculated as described in Ref. 29.

N	$f_{2e}/f_{1e}^{(a)}$ (Singlet)	$f_{2e}/f_{1e}^{(a)}$ (Triplet)
10	1.71 [55]	1.86 [45]
12	1.78 [78]	1.92 [66]
15	1.85 [120]	1.94 [90]
20	1.92 [210]	1.95 [190]

TABLE II: Verification of the oscillator strength sum rule for the calculated spectroscopy of singlet and triplet dielectrons. The numbers reported are the ratios of the oscillator strength of a singlet or triplet dielectron to the oscillator strength of a (single) hydrated electron (see Section IV). The numbers in brackets are the number of product–basis states that can be formed from N single–electron eigenstates. The table is truncated at N=20 because our block–Lanczos solver runs into numerical trouble for N $\geq$ 21.

FIG. 1: Singlet and triplet dielectron charge densities with their first–solvation shell of water molecules, for representative singlet and triplet configurations. The blue charge–density contours are contours of 10% of the maximum dielectron charge density, and the water molecules are drawn in the CPK representation using the program *gOpenMol* (Ref. 22). For clarity, we have removed two water molecules in front of the triplet dielectron.

FIG. 2: Decomposition of a singlet dielectron wave function into product–basis states for a representative singlet–dielectron/water configuration. The wire mesh in each panel is drawn for a contour at 10% of the maximum charge density of this singlet dielectron. The solid contours on the left, from top to bottom, are drawn at 10% of the charge density maximum for the first, second, and fifth single–electron states for this water configuration. The solid contours in the right column display, from top to bottom, the 10% charge–density–maximum level of the three two–electron product–basis states that contribute the most to the singlet dielectron wavefunction for this water configuration: $|1,1>_+$, $|2,2>_+$, and $|1,5>_+$ (see Section II A).

FIG. 3: Radial distribution functions for the distance between the singlet dielectron center–of–mass and various water sites, computed from a 30–ps equilibrium molecular dynamics simulation using configurations sampled every 30 fs, for a total of 1000 dielectron/water configurations. The solid curve represents the dielectron/oxygen radial distribution function and the dashed curve represents the dielectron/hydrogen distribution.

FIG. 4: Contour plots of the cylindrical distribution function of distances between the triplet dielectron and various water sites, computed using Eq. 8 as described in Section III A 2. The distribution was generated from a 30–ps equilibrium molecular dynamics simulation using configurations sampled every 30 fs, for a total of 1000 dielectron/water configurations. The spacing between contours is 0.2, with a maximum value of 1.8. The upper panel is for hydrogen sites, the middle panel for oxygen sites, and the lower panel is the net site density (a 2/3:1/3 weighted sum of the upper and middle panels). The white contour in the middle panel replicates the $g_{cyl} = 0.8$ contour from the upper, hydrogen–site, panel. Note that the way we calculate g_{cyl} guarantees perfect symmetry on reflection about the $z = 0$ axis; the slight asymmetries are artifacts of the program used to draw the contours.

FIG. 5: Dynamical history of various properties of the singlet dielectron. The upper panel shows various dielectron energies: the lowest solid black curve is the dielectron ground–state energy, E_1; the gray curve is the first excited–state energy, E_2; the upper solid curve is the Coulomb energy, V_C; and the dashed curve is the exchange energy, V_{ex}. The lower panel displays two geometric properties of the singlet dielectron, the radius of gyration, R_{gyr} (Eq. 4, black curve) and the root–mean–squared separation, r_{12} (Eq. A2, gray curve).

FIG. 6: Dynamical history of various properties of the triplet dielectron. The upper two panels show the same properties as the two panels of Fig. 5 and use the same convention for all curves. The bottom panel displays the root–mean–squared separation, r_{12} (Eq. A2), for the full 30 ps calculations. Note the two failed dissociation attempts at $\sim$5 ps and $\sim$20 ps.

FIG. 7: Autocorrelation functions of singlet dielectron quantum energies: the ground state energy (E_1, solid black curve); the ground–to–first–excited–state energy gap (E_{12}, dash–dotted curve); the Coulomb energy (V_C, dashed curve); and the exchange energy (V_{ex}, solid gray curve).

FIG. 8: Autocorrelation functions for the singlet dielectron geometry: the radius of gyration, Eq. 4 (R_{gyr}, solid black curve); the root–mean–squared separation, Eq. A2, (r_{12}, dashed curve); and the symmetry order parameter, Eq. 6 (η, solid gray curve).

FIG. 9: Autocorrelation functions of triplet dielectron quantum energies, plotted using the same conventions as in Fig. 7.

FIG. 10: Autocorrelation functions for the triplet dielectron geometry, plotted using the same conventions as in Fig. 8.

FIG. 11: Equlibrium optical absorption spectra for singlet dielectrons (solid black curve), triplet dielectrons (dashed curve), and for the (single) hydrated electron (solid gray curve). The singlet and triplet dielectron spectra were calculated from Eq. 10 using 10,000 configurations (sampled every 3 fs from the 30–ps molecular dynamics runs described in Section II). The (single) hydrated electron absorption spectrum was computed using a one–electron analog of Eq. 10, with the lowest ten single–electron adiabatic eigenstates from each configuration; this calculation used 5000 configurations, separated by 1 fs, from a 5–ps run.

FIG. A1: Correlation of electron–electron interactions with the root–mean–squared separation, r_{12} (Eq. A2), for singlet (upper panel) and triplet (lower panel) dielectrons. Each point plots the Coulomb energy, V_C (+), the exchange energy, V_{ex} ($\times$), or their sum ($*$) versus r_{12}, with the points for both the singlet (upper panel) and the triplet (lower panel) dielectron sampled every 3 fs from the 30–ps molecular dynamics simulations described in Section II.

Singlet dielectron

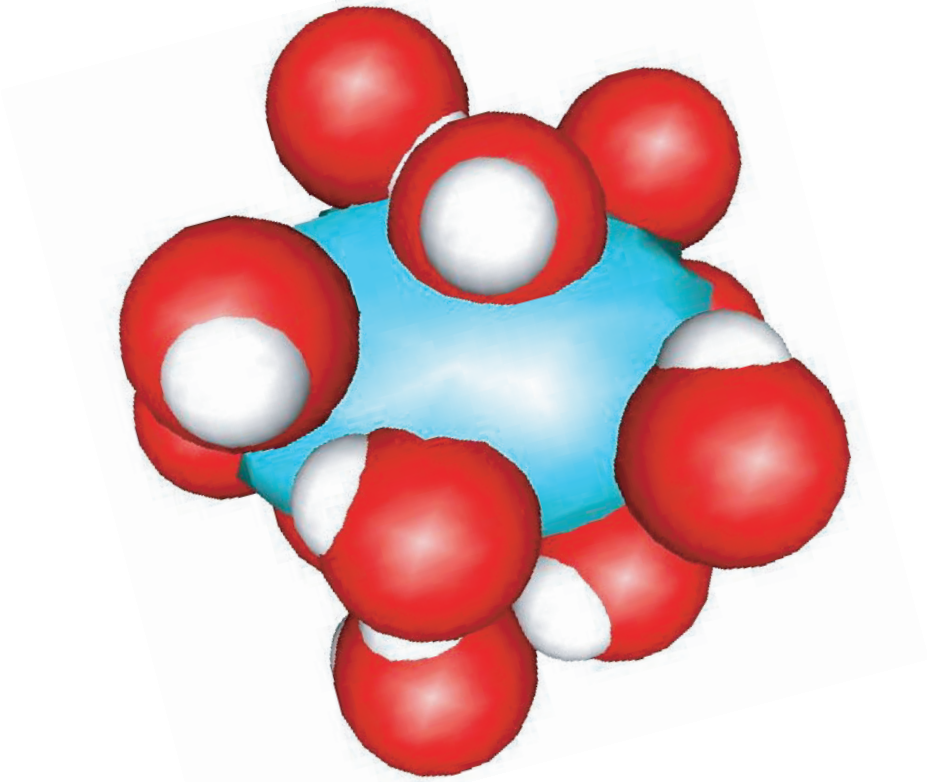

Triplet dielectron

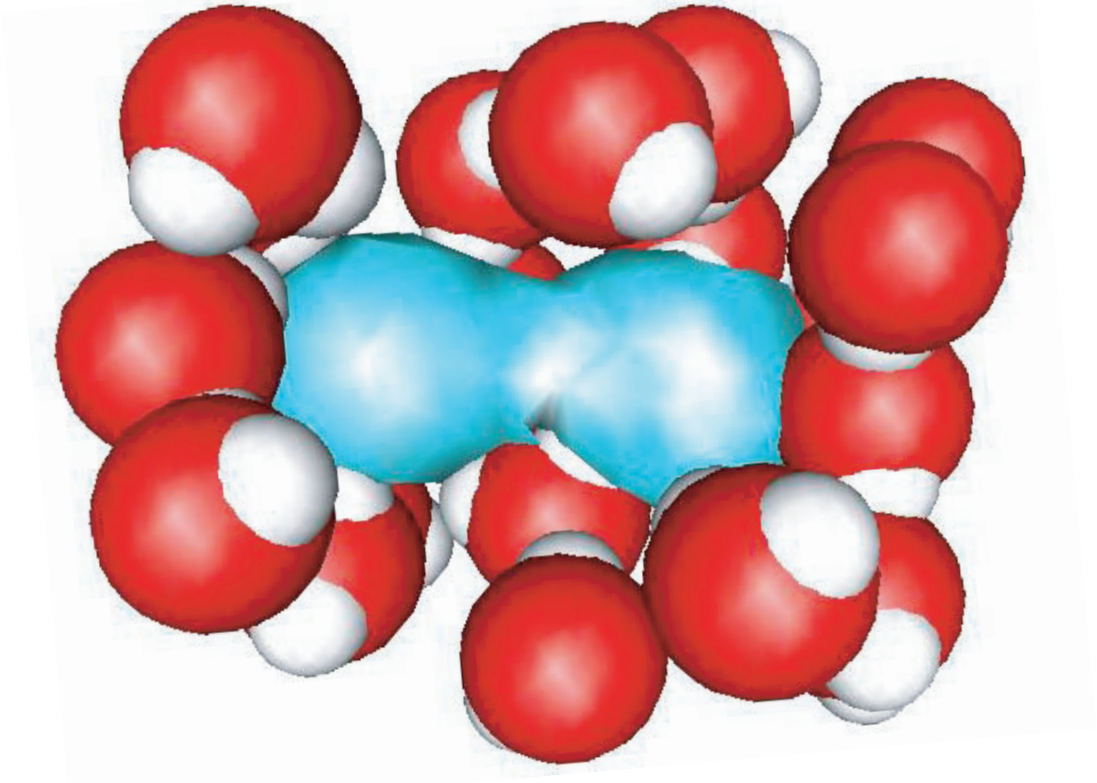

Larsen and Schwartz, Fig. 1

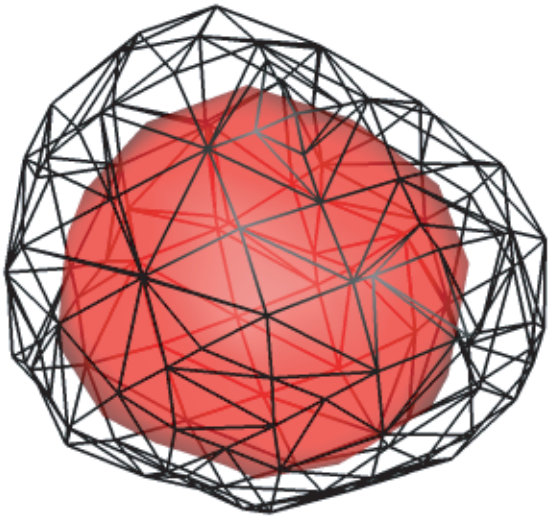

|1>

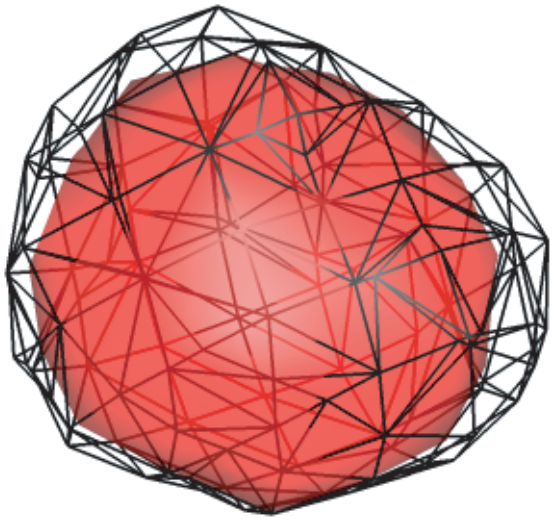

|1,1>+

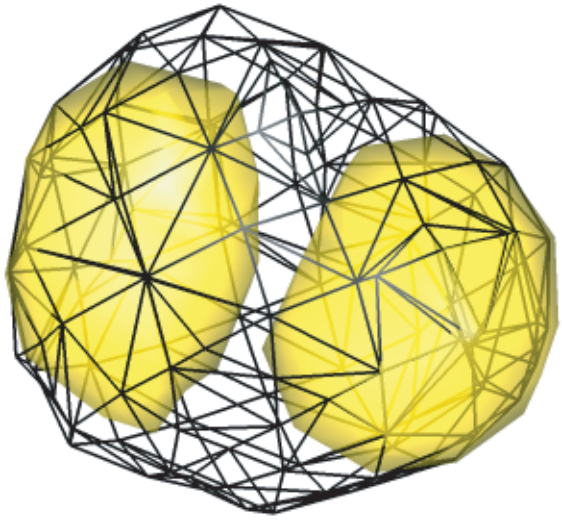

|2>

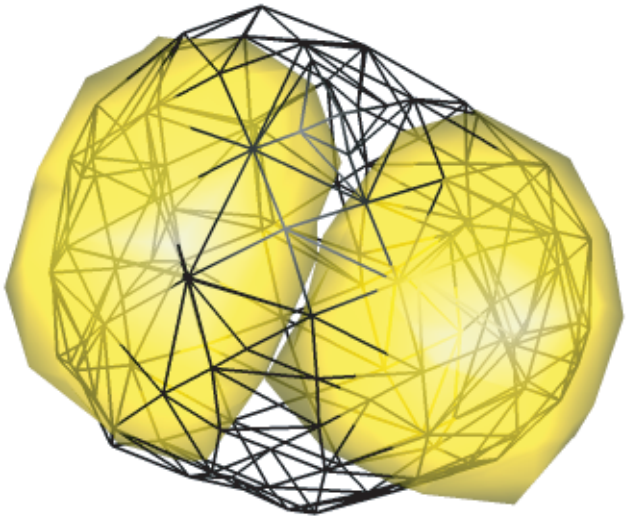

|2,2>+

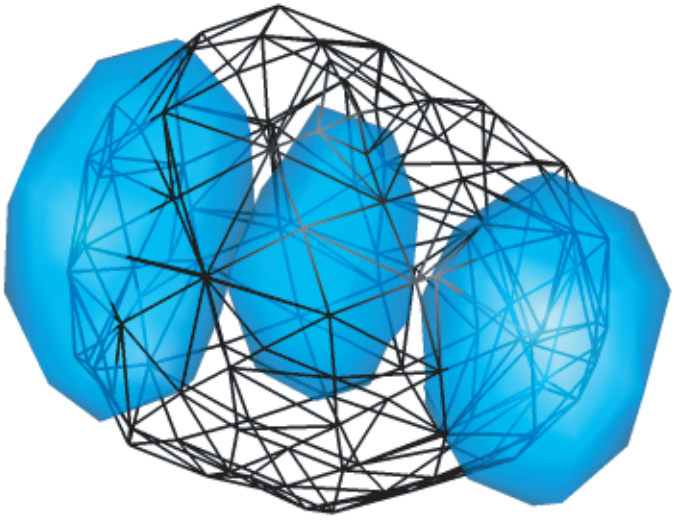

|5>

|1,5>+

Larsen and Schwartz, Fig. 2

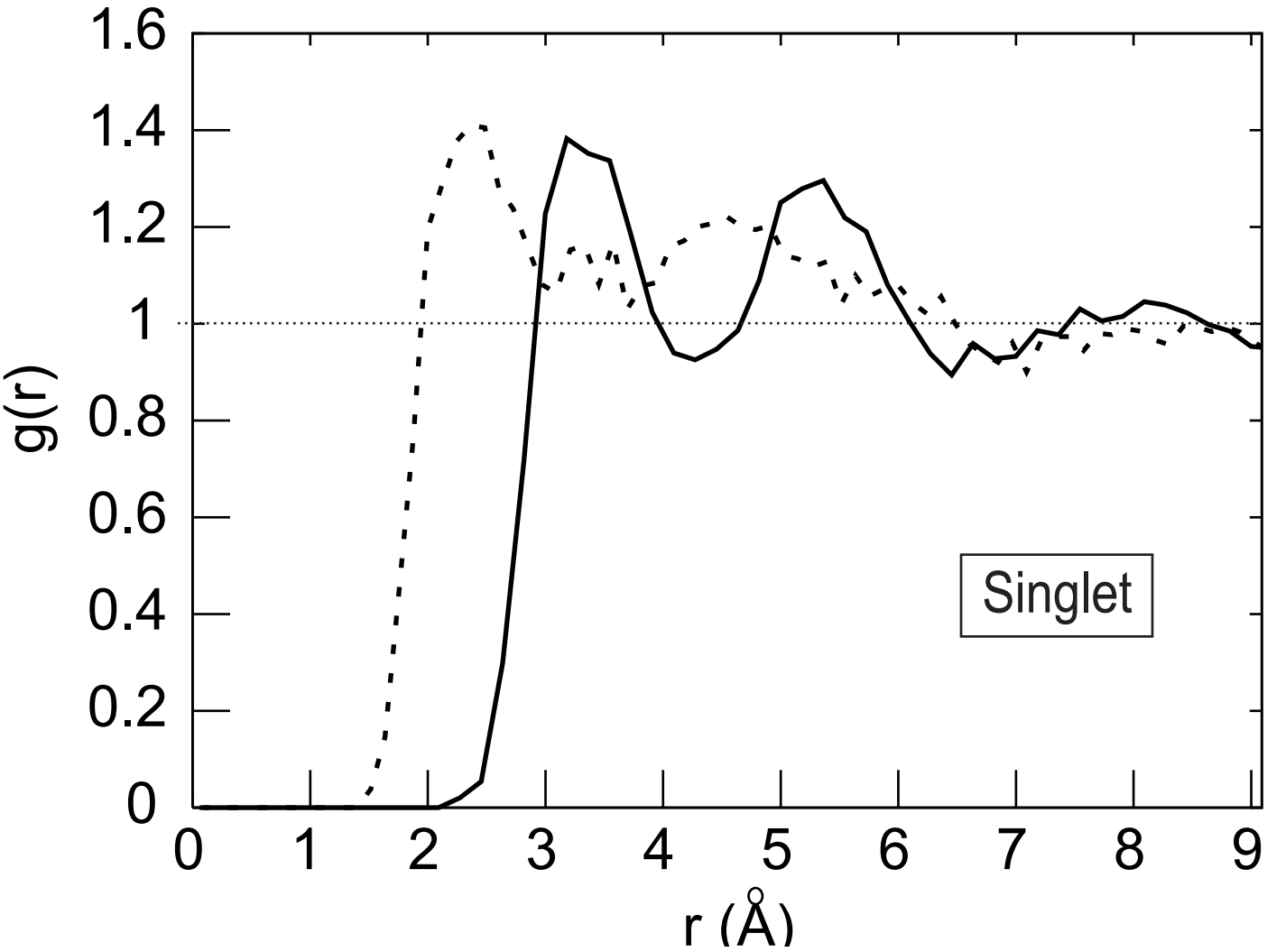

Larsen and Schwartz, Fig. 3

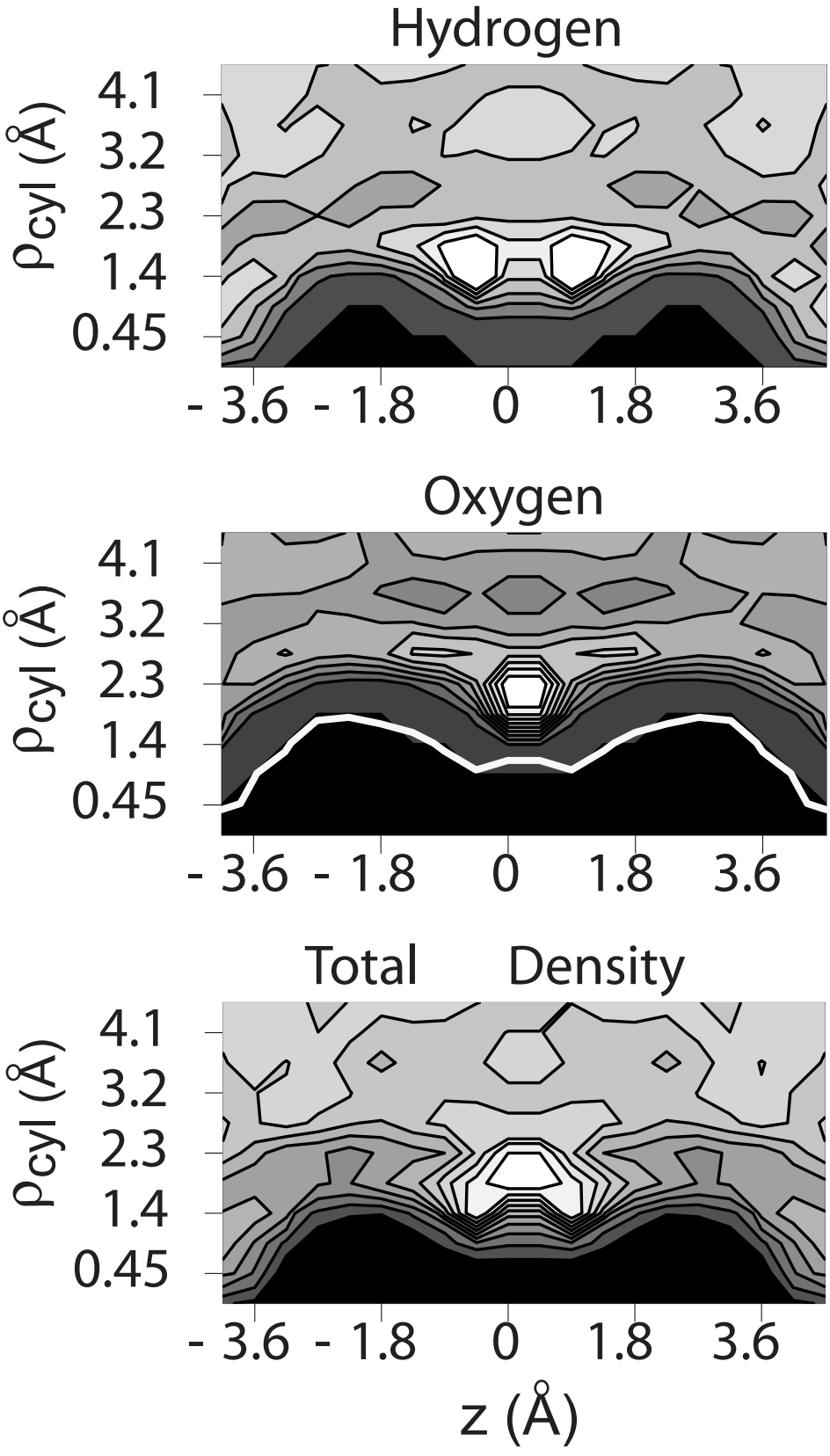

Larsen and Schwartz, Fig. 4

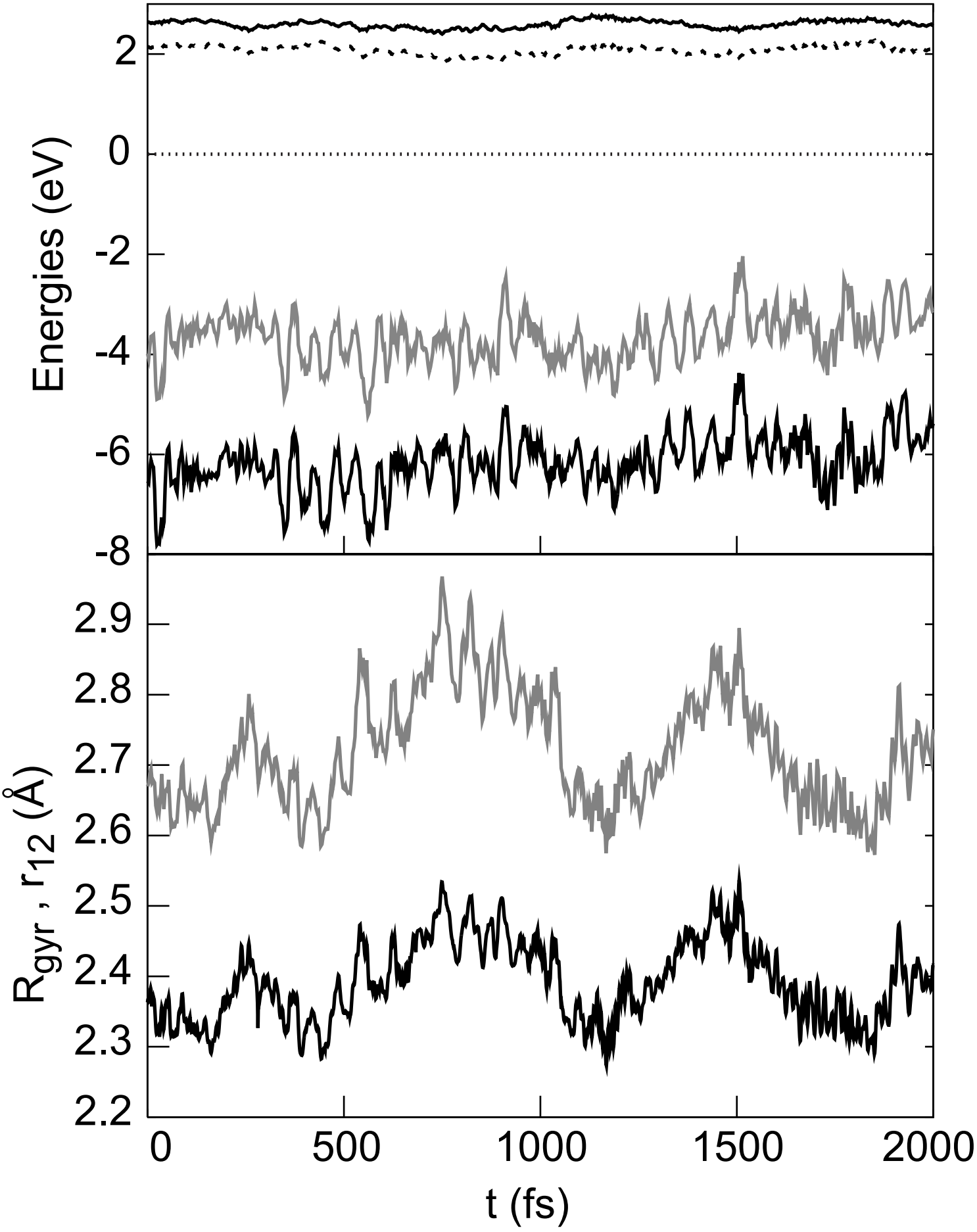

Larsen and Schwartz, Fig. 5

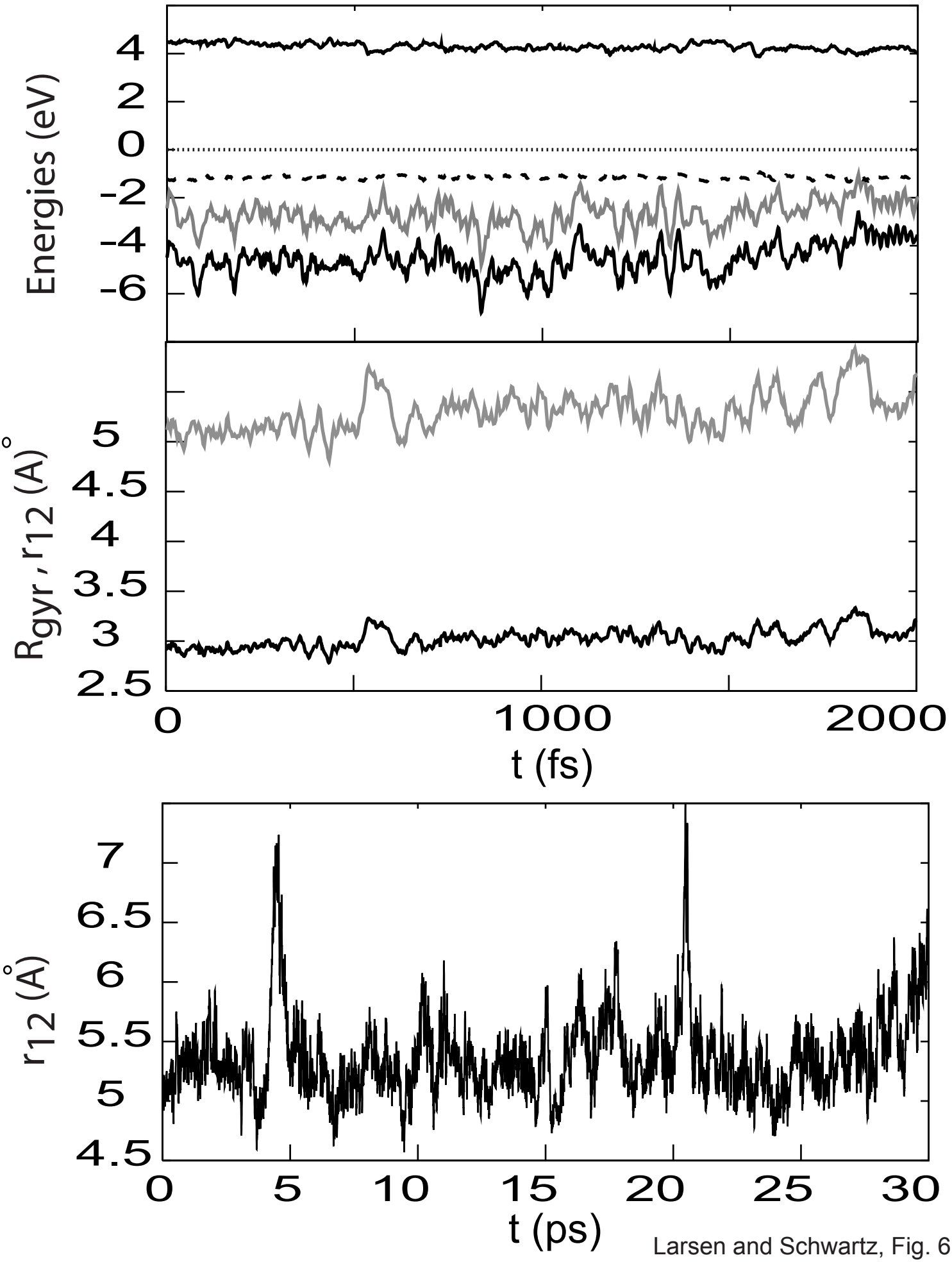

Larsen and Schwartz, Fig. 6

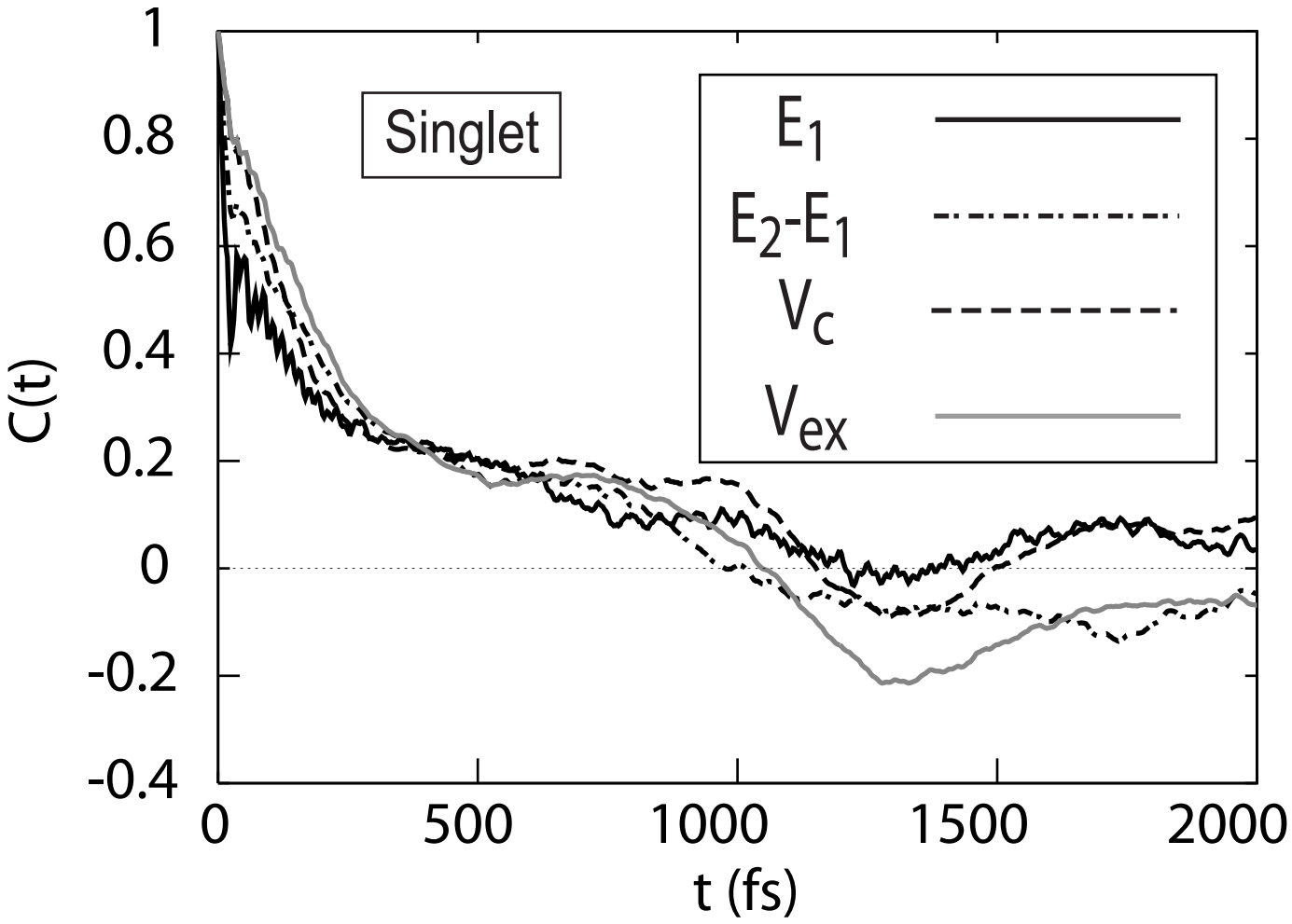

Larsen and Schwartz, Fig. 7

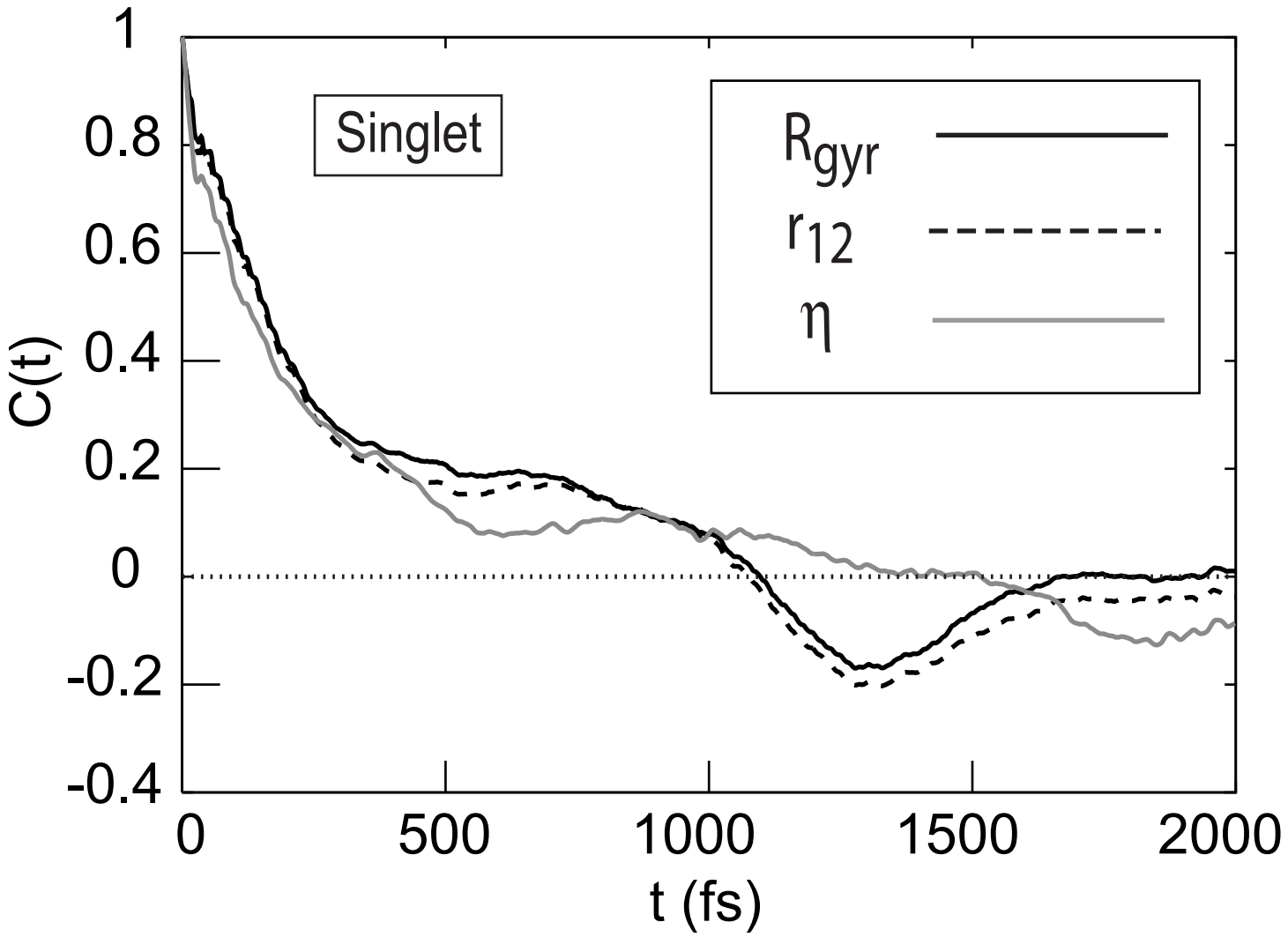

Larsen and Schwartz, Fig. 8

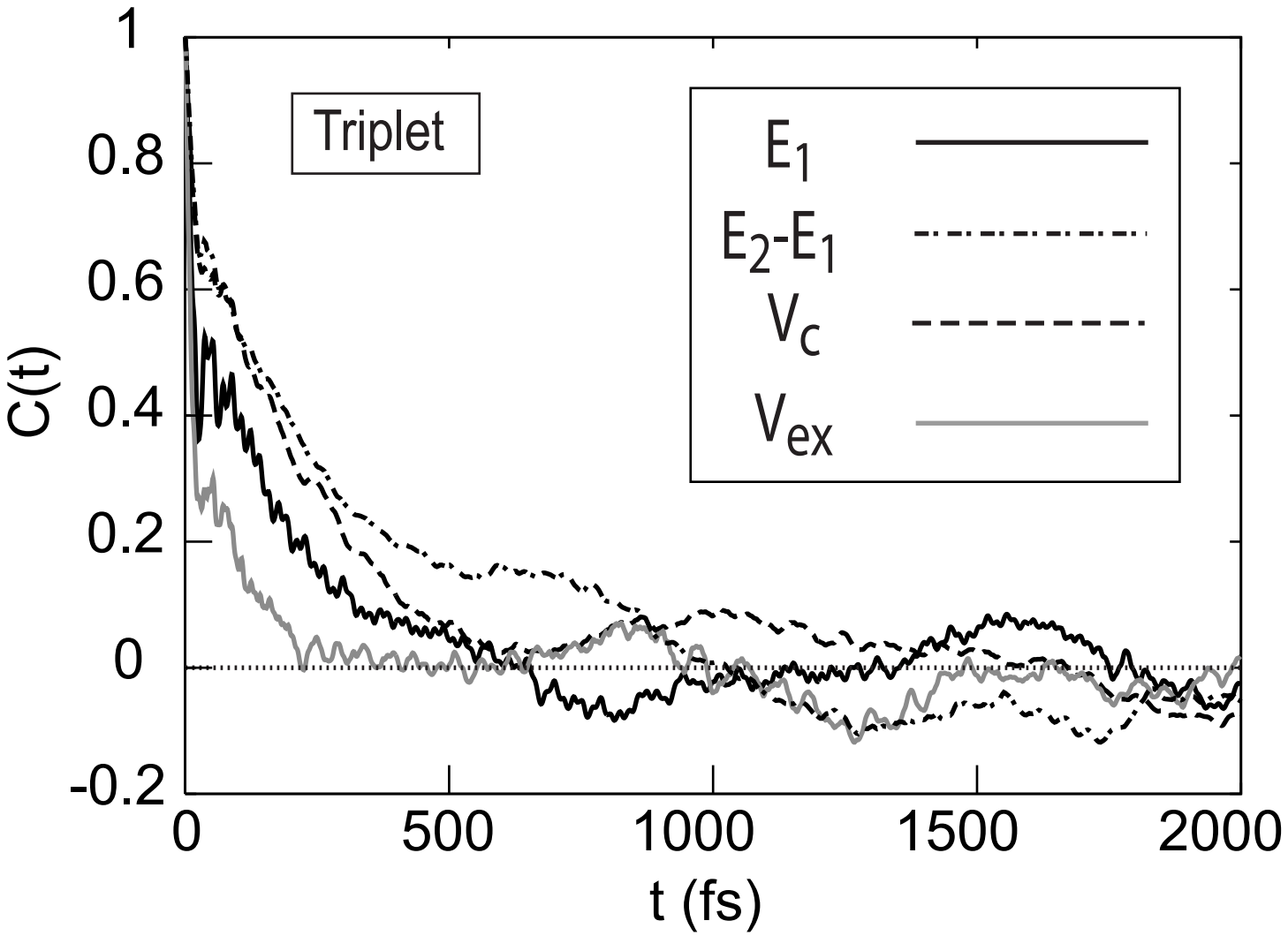

Larsen and Schwartz, Fig. 9

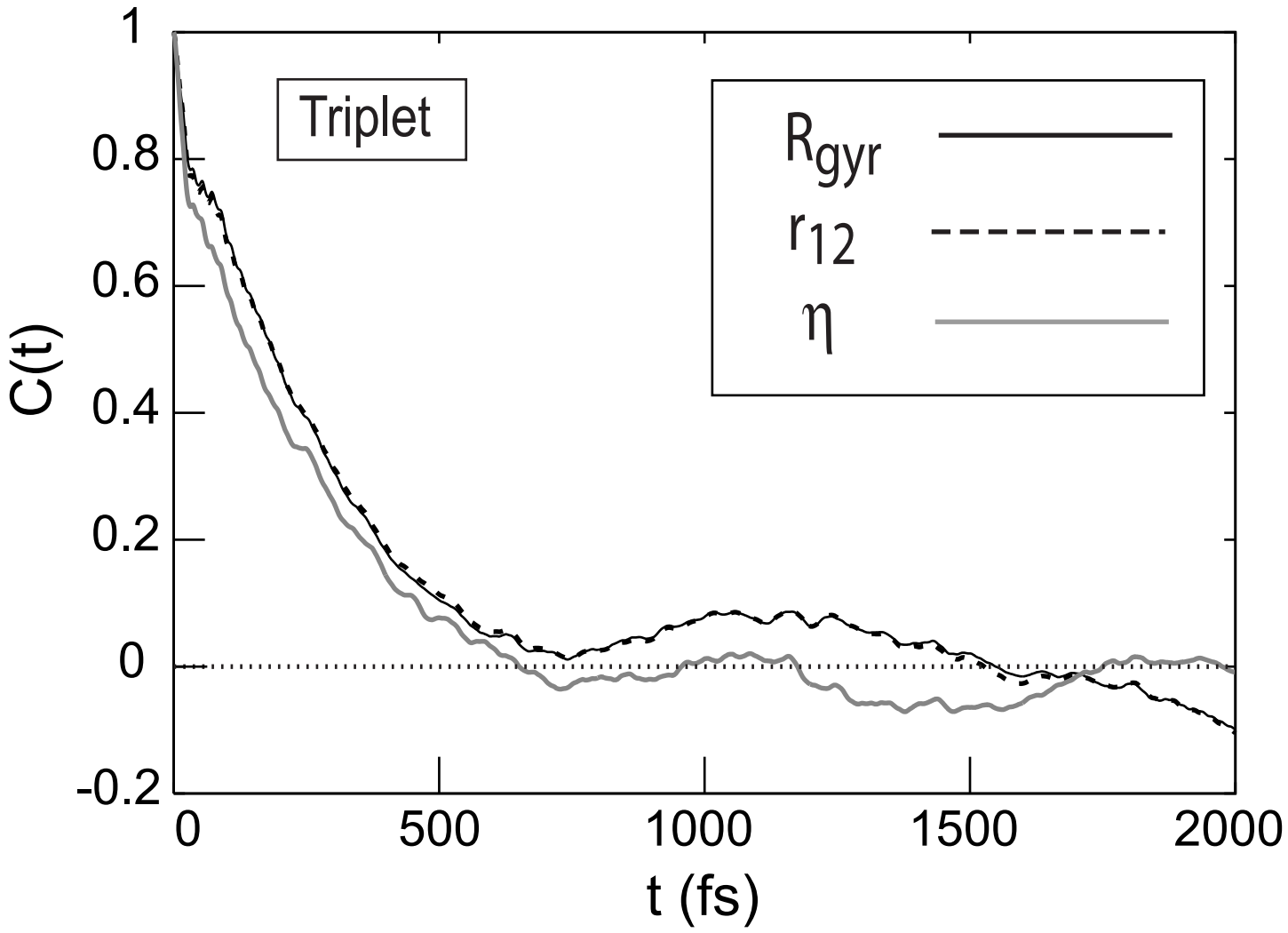

Larsen and Schwartz, Fig. 10

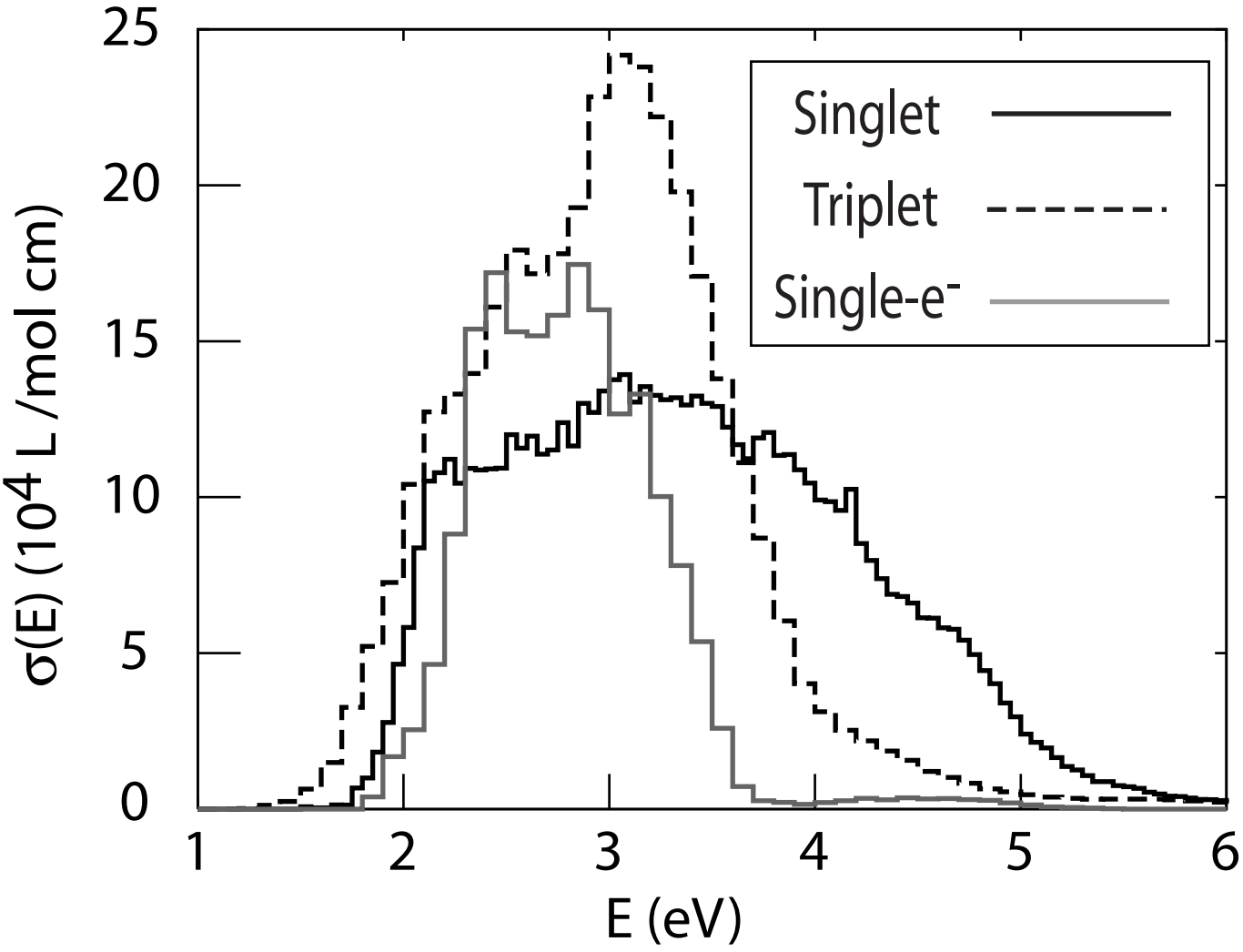

Larsen and Schwartz, Fig. 11

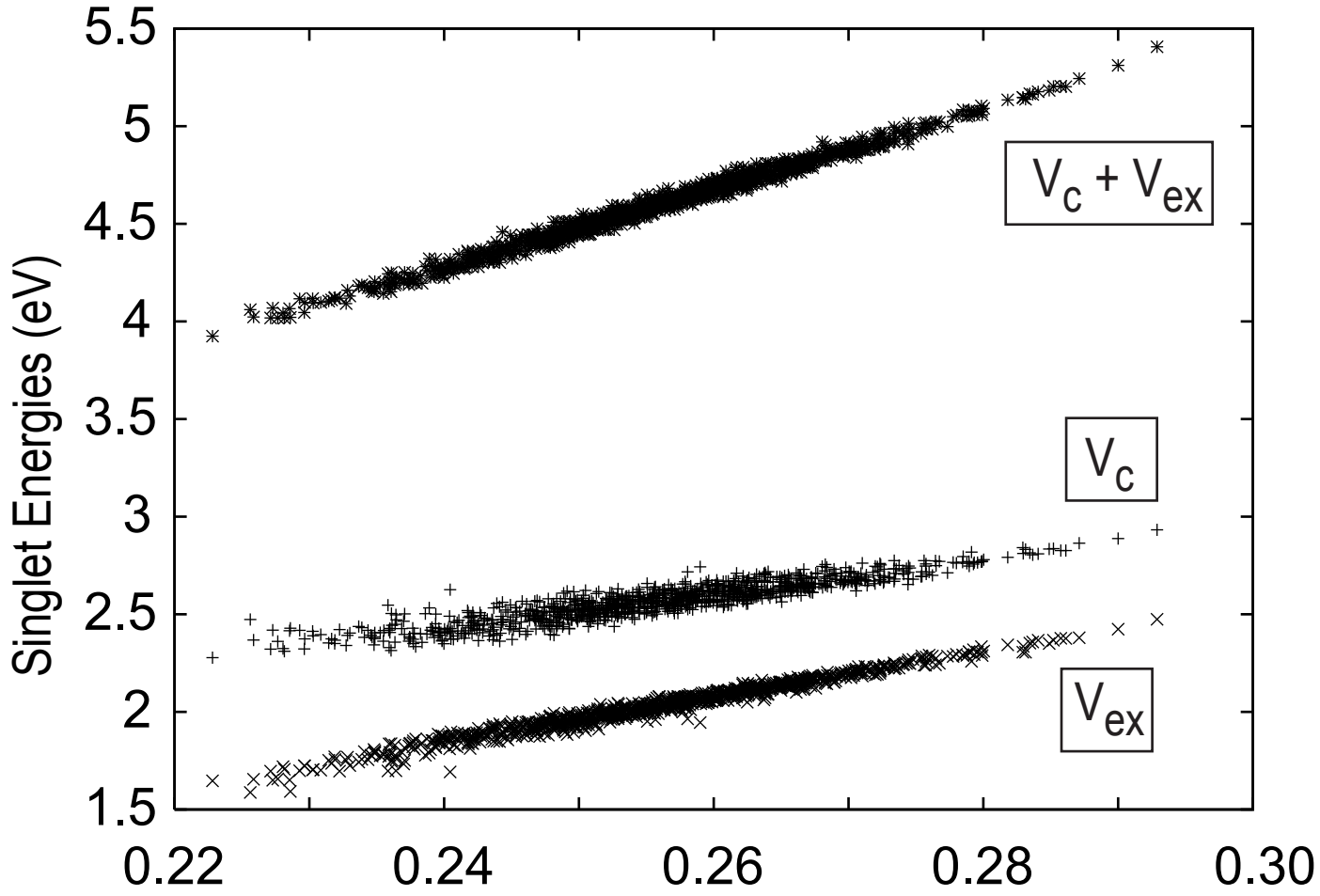

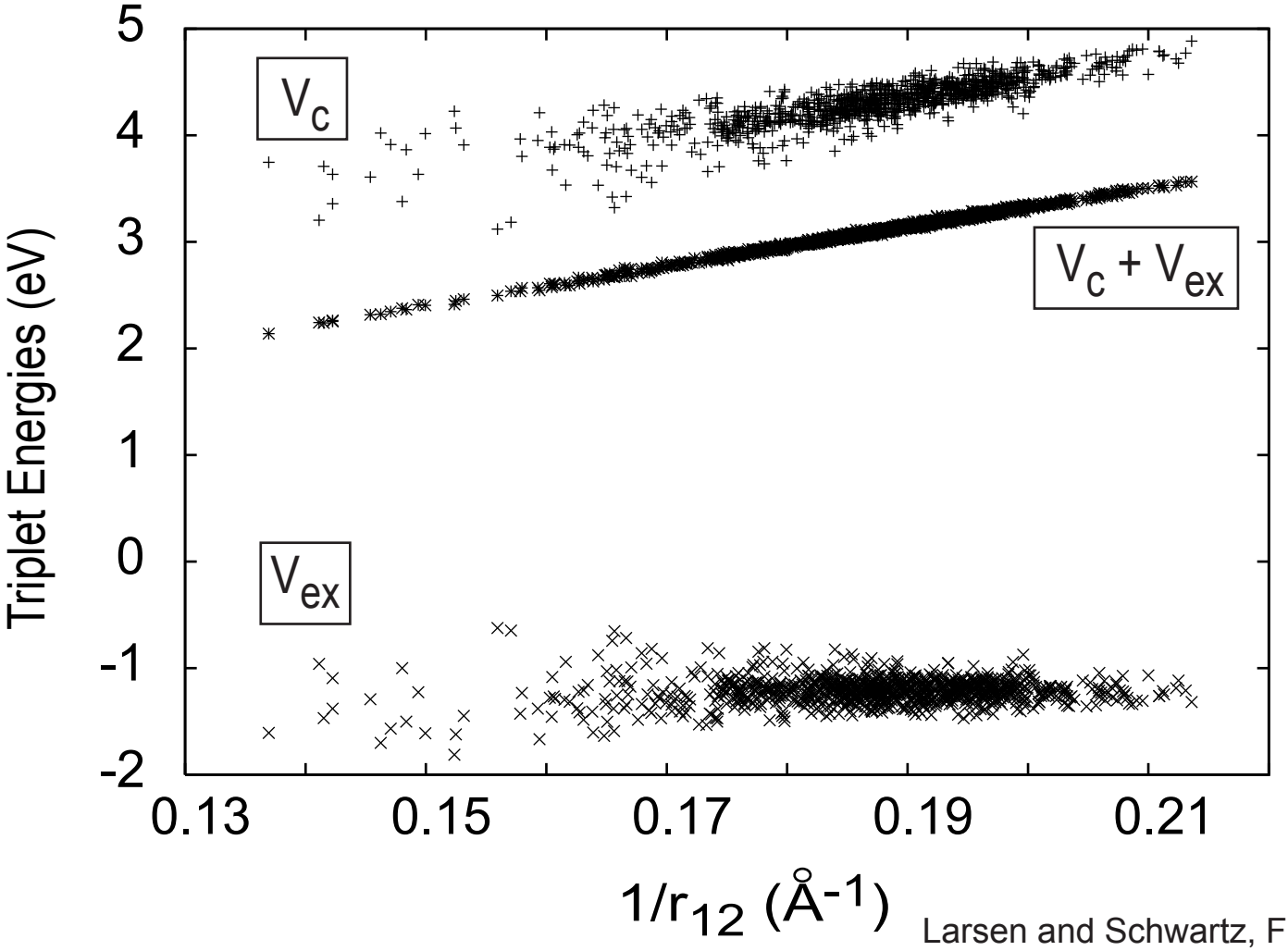

Larsen and Schwartz, Fig. A1